

A Novel Transmission Policy for Intelligent Reflecting Surface Assisted Wireless Powered Sensor Networks

Zheng Chu, *Member, IEEE*, Pei Xiao, *Senior Member, IEEE*, De Mi, *Member, IEEE*, Wanming Hao *Member, IEEE*
Mohsen Khalily, *Senior Member, IEEE*, and Lie-Liang Yang, *Fellow, IEEE*

Abstract—This paper proposes a novel transmission policy for an intelligent reflecting surface (IRS) assisted wireless powered sensor network (WPSN). In particular, an energy station (ES) broadcasts energy wirelessly to multiple sensor nodes, which transmit their own information to an access point using the harvested energy. An IRS is deployed to enhance the performance of wireless energy transfer (WET) and wireless information transfer (WIT) by intelligently adjusting phase shifts of each reflecting elements. To achieve its self-sustainability, the IRS needs to collect energy from the ES to support its control circuit operation. Our proposed policy for the considered WPSN is called *IRS assisted harvest-then-transmit time switching (IRS-HTT-TS)*, which is able to schedule the transmission time slots by switching between energy collection and energy reflection modes. We study the performance of the proposed transmission policy in terms of the achievable sum throughput, and investigate a joint design of the transmission time slots, the power allocation, as well as the discrete phase shifts of the WET and WIT. This formulates the problem as a mixed-integer non-linear program (MINLP), which is NP-hard and non-convex. To deal with this problem, we first relax it to the one with continuous phase shifts, and then propose a two-step approach and decompose the original problem into two sub-problems. We solve the first sub-problem with respect to the phase shifts of the WIT in terms of closed-form expression. Next, we consider two cases to solve the second sub-problem. Specifically, for the special case without the circuit power of each sensor node, the Lagrange dual method and the Karush-Kuhn-Tucker conditions are applied to derive the optimal closed-form transmission time slots, power allocation, and phase shift of the WET. Moreover, we exploit the second sub-problem for the general case with the circuit power of each sensor node, which can be solved via employing a semi-definite programming relaxation. The optimal discrete phase shifts can be obtained by quantizing the continuous values. Numerical results demonstrate the effectiveness of the proposed policy and validate the beneficial role of the IRS in comparison to the benchmark schemes.

Index Terms—Wireless powered sensor network, internet of things, time switching, intelligent reflecting surface, phase shift.

I. INTRODUCTION

Massive connectivity and ultra-high data rate have been two of important pillars in the future generation of communication networks [1]. On the other hand, internet of things (IoT) is typically considered as a significant portion of future wireless networks to guarantee multiple types of connectivities for massive IoT devices in a highly spectral/energy efficient fashion [2], [3]. For a generic IoT system, multiple wireless devices (WDs) (e.g., sensor nodes) establish low-power transmission links to an access point (AP), forming a wireless sensor network (WSN). This has been widely applied to various

vertical industries, e.g., event detection of emergency services, structural health monitoring, healthcare diagnosis. [4]. In practice, these WDs are very likely to be powered by the finite-capacity battery, and consequently barely have sufficient energy to support their own computational and communication operations. Traditional ways of battery maintenance and replacement can be often costly and sometime infeasible, especially for massive WDs placed in extreme environments, infrastructures, or human bodies [5]. Thus, the WDs working with a limited battery lifetime is still a bottleneck for future multiple access wireless networks.

In recent years, radio frequency (RF) wireless energy transfer (WET) has been considered to tackle the energy-constrained issue by novel electromagnetic energy harvesting in a wireless fashion [5]–[8]. Wireless powered communication network (WPCN) has emerged as one of the promising WET solutions to ensure a stable energy supply. It relies on dedicated energy sources (ESs) to provide wireless charging for the WDs via RF WET, such that these WDs have sufficient power to support their wireless information transfer (WIT) [9], [10]. The WPCN adopts a generic protocol called “*harvest-then-transmit*” to schedule the WET and WIT transmission time slots to circumvent the potential interference [11]. Also, the WPCN can benefit from the extended WDs’ operational lifetime via wireless charging and from the reduced maintenance cost. Thus, the WPCN is a viable solution for the low power consumption devices to form a wireless powered sensor network (WPSN) [4].

On the other hand, various advanced techniques have been developed to improve the achievable data rate, e.g., relaying, massive multiple-input multiple-output (massive MIMO), ultra-dense networks (UDNs), millimetre wave (mmWave) and Terahertz (THz) communications [12]–[14]. However, these techniques always incur very high energy consumption and hardware cost, since a large amount of RF chains are used at the transmitter over a high frequency band, and thus more transmitted data requires more emission of radio waves [15], [16]. This has driven the development of a novel and promising paradigm, named *smart and reconfigurable radio environment*. It is a *holographic* wireless mode with an unconventional hardware architecture which features low cost, small size, light weight and low power consumption [17]. *Smart and reconfigurable radio environment* potentially provides a seamless wireless connectivity and the capabilities of transmitting and processing data by recycling the existing radio waves

rather than generating new ones, which is a transformative way to convert the traditional wireless environment into a programmable intelligent entity [15]–[17]. As a key enabler of *smart and reconfigurable radio environment*, intelligent reflecting surface (IRS) (also known as reconfigurable intelligent surface (RIS)), has been proved to effectively improve the spectral and energy efficiencies of wireless systems [18]. The IRS consists of a large number of reconfigurable reflecting elements, which are managed by a smart controller. These elements possess small-size, low-cost, and low-energy consumption features, and can help strengthen the signal reception by intelligently adjusting the desired signal phase without a dedicated RF processing, en/de-coding, or re-transmission [19].

A. State-of-the-Art

1) *IRS Assisted Wireless Networks*: Recently, variety of research contributions focus on the IRS-enabled wireless networks [20]–[33]. In [20], an IRS assisted multiple-input single-output (MISO) downlink system was proposed to jointly optimize the active transmit beamforming of the base station (BS) and passive reflecting beamforming generated by the IRS. The minimization problem of the total transmit power is resolved by an alternating optimization (AO) algorithm to suggest the beneficial role of the IRS in improving power efficiency compared with the traditional schemes. The work in [21] considered a similar system and maximized its energy efficiency such that the power allocation and the phase shifts of the IRS are optimally designed by the AO algorithm, gradient descent search, and sequential fractional programming. The integration of IRS with wireless security has been considered in [22]–[24]. The IRS is introduced to reduce the power consumption and enhance the achievable secrecy performance via alternately designing the active secure transmit and passive reflecting beamformers [22], [23]. It was shown in [24] that the use of artificial noise (AN) is beneficial to enhance the achievable secrecy rate of an IRS assisted downlink secure system in comparison to its counterparts without IRS or AN. In [25], the IRS is deployed to assist a multi-cell MIMO system, where the edge users can benefit from such a system deployment to mitigate the inter-cell interference. In addition, a block coordinate descent (BCD) algorithm is proposed in [25] to solve the formulated weighted sum rate (WSR) maximization, which jointly designs the transmit precoding matrices and phase shifts. The Majorization-Minimization (MM) algorithm and the complex circle manifold (CCM) method are adopted to design the locally optimal phase shifts. Moreover, an IRS-assisted multigroup multicast system was investigated in [26], where a multi-antenna BS broadcasts independent data streams to multiple groups. All single-antenna users in the same group receive the same information, and the inter-group interference is incurred. The second-order cone programming (SOCP) is considered to solve the sum rate maximization of all multicasting groups, and a low complexity algorithm is designed to derive the closed-form solutions of the transmit beamforming and phase shifts. Moreover, the IRS is deployed for not only information reflection to assist the direct link, but also the

energy reflection to improve the self-sustainability of wireless networks. The IRS assisted simultaneous wireless information and power transfer (SWIPT) has been investigated in [27], [28]. In [27], by solving the maximization of the weighted harvested energy of energy harvesting users (ERs) subjecting to the individual signal-to-interference-plus-noise ratio (SINR) constraint for information decoding users (IRs), the WET efficiency is enhanced and the rate-energy trade-off is characterized for the IRS enabled SWIPT system. Furthermore, multiple IRSs are deployed to support the information/energy transfer from an access point (AP) to IRs as well as ERs [28]. The minimization problem of the total transmit power is iteratively solved by an efficient penalty-based method, which demonstrates the effect of IRSs on the energy efficiency enhancement. In [29], the maximization problem of the WSR of the IRs was studied for an IRS assisted MIMO SWIPT system, guaranteeing the energy harvesting requirement of the ERs. The IRS is integrated in the mmWave and THz communications over orthogonal frequency division multiple access (OFDMA) in [30], where the WSR is maximized for the design of the hybrid analog/digital beamforming at the BS and passive beamforming at the IRS. In addition, a more practical case was exploited with imperfect channel state information (CSI), and a robust beamforming and reflecting phase shift matrix are designed to solve the formulated WSR maximization problem. An exact coverage analysis of IRS has been investigated with generic Nakagami-m fading channels [31], where a moment generation functions (MGF) based framework was developed to characterize the coverage probability. Joint design for the communication and computing is a promising paradigm [32], which fits within the IRS assisted wireless networks to improve offloading efficiency. In [33], RIS, as an option of new physical layer techniques beyond fifth-generation (5G) network, has been overviewed, where three challenges on the controllable wireless environment, better asymptotic array gains, as well as the path loss of the cascaded channel has been unveiled. In addition, two critical questions on use cases and channel estimation with real-time feedback have been unlocked to safeguard the success of RIS.

2) *Wireless Powered Communication Network*: On the other hand, there has been various research endeavours that investigated WPCN [11], [34]–[38]. In [11], the concept of WPCN was proposed, where the dedicated energy supply radiates wireless energy to the energy-constrained users that utilize harvested energy to support information transmissions. Recently, a novel non-linear energy harvesting model was characterized [34], where the relation between the direct current (DC) and the received RF signal power was exploited based on its convex property. In [35], a MIMO WET system was investigated to enlarge the output DC power by jointly optimizing the multi-sine waveform and beamforming. It was shown that the proposed scheme offers a higher output DC power than the only beamforming design. In [36], the impact of the WPCN was studied in the static and mobile coexisting networks, where the total received power and the throughput achieved by the energy harvesting node were characterized. Ambient RF energy harvesting was considered as an enabler of wireless powered IoT networks [37], which exploited the

packet transmission in grant-free opportunistic uplink WIT charged by the downlink WET. Very recently, new challenges and opportunities for the WET were introduced for future wireless networks to take full advantage of the RF radiations and spectrum in providing cost-effective and real-time power supplies to wireless devices and enable wireless powered applications [38]. The benefits of IRS to WET arise from the fact that IRS can help increase the RF power level at the input of the rectenna. Thus, the synergy between IRS and WPCN forges a promising solution to improve the energy/information reflection efficiency. Particularly, an IRS was considered in [39] to improve wireless data aggregation in an over-the-air computation (AirComp) system, where the minimization problem of the mean-squared-error (MSE) is formulated to jointly design energy and aggregation beamformers at the AP, downlink/uplink phase-shifts at the IRS, and transmit power at the IoT devices, quantifying the AirComp distortion.

Although the existing works made variety of research contributions in the IRS aided wireless networks, and the IRS aided SWIPT systems, there still exists a major research gap on investigation of the IRS's benefits in a WPSN. Specifically, utilizing IRS to enhance energy harvesting and data transmission capabilities of the WPSN due to its self-sustainability, has not yet been investigated in the existing works. Furthermore, the IRS can be considered to properly coordinate the energy/information RF signals to offer an coverage enhancement for downlink wireless charging and uplink throughput improvement for the WPSN. Moreover, in the existing works, it is assumed that the IRS does not require any energy for its own circuit operation. However, the IRS controller typically coordinates the channel estimation mode and the data reflection mode [20], necessitating the sufficient energy for circuit operation. To the best of the authors' knowledge, there is few of work having exploited the transmission policy for the IRS aided WPSN, which motivates this paper.

In this paper, a novel transmission policy of a IRS assisted WPSN is proposed, where the IRS helps multiple sensor nodes to enhance their energy harvesting efficiencies and data transmission capabilities, and simultaneously maintain its own circuit operation. *The main contributions of this paper are highlighted as follows.*

- 1) We exploit an IRS assisted WPSN system, to be specific, an ES provides WET to multiple sensor nodes, which in turn utilize the collected energy to support their WIT via the time division multiple access (TDMA). Also, the IRS is deployed to improve energy reception at the sensor nodes and information reception at the AP, apart from maintaining its own circuit energy consumption. An *IRS assisted harvest-then-transmit time switching* (IRS-HTT-TS) transmission policy is proposed to efficiently schedule the transmission time slots of the WET and WIT phases.
- 2) To evaluate the performance of the IRS assisted WPSN, we aim to maximize the sum throughput subject to the power constraints of individual sensor node and the IRS, the transmission time constraints, the constraint of the discrete phase shifts. Due to quantized phase

shifts, the formulated problem is a mixed-integer non-linear program (MINLP), which is an NP-hard problem. We first relax it into its counterpart with continuous phase shifts which is still a non-convex problem due to multiple coupled variables.

- 3) To deal with the non-convex issue, we propose a two-step approach to decompose the relaxed problem into two sub-problems, which can be solved separately. First, we independently solve the first sub-problem to derive the optimal close-form phase shifts of the WIT. Then, we consider two cases to solve the second sub-problem: a special case and a general case. For the special case without circuit power of each sensor node, we exploit the Lagrange dual method and Karush-Kuhn-Tucker (KKT) conditions to derive the optimal closed-form transmission time slots, power allocation, and phase shift of the WET. Moreover, we resolve the second sub-problem for the general case with the circuit power of each sensor node, which can be solved by taking into consideration a semi-definite programming (SDP) relaxation. Consequently, the optimal discrete phase shifts can be obtained by quantizing the continuous counterparts.

The rest of this paper is organized as follows. The system model and the proposed *IRS-HTT-TS* transmission policy are described in Section II. Section III investigates the sum throughput maximization for the IRS assisted WPSN. Section IV provides numerical results to evaluate the proposed algorithm. Finally, we conclude this paper in Section V.

B. Notations

We use the upper case boldface letters for matrices and lower case boldface letters for vectors. $\text{conj}(\cdot)$, $(\cdot)^T$ and $(\cdot)^H$ denote the conjugate, the transpose and conjugate transpose operations, respectively. $\text{Tr}(\cdot)$ stands for trace of a matrix. $\mathbf{A} \succeq \mathbf{0}$ indicates that \mathbf{A} is a positive semidefinite matrix. $|\cdot|$ and $\|\cdot\|$ denote the absolute value and the Euclidean norm of a vector. $\exp(\cdot)$ and $\arg(\cdot)$ indicate the exponential function and the phase operation, respectively. $\mathcal{W}(\cdot)$ denotes the Lambert \mathcal{W} function. $\Re\{\cdot\}$ represents the real part of a complex number. $\text{diag}\{\cdot\}$ denotes a diagonal matrix. $x \in \mathcal{CN}(0, 1)$ denotes that x follows the complex Gaussian distribution with zero-mean and unit variance.

II. SYSTEM MODEL

In this section, we consider an IRS assisted WPSN as shown in Fig. 1, which is composed of a single-antenna ES, a single-antenna AP, K IoT sensor nodes as well as an IRS with N_R passive reflecting elements. Specifically, the ES, connected with a stable microgrid for energy supply, provides wireless charging service to the sensor nodes, that can utilize the harvested energy to transmit their own message

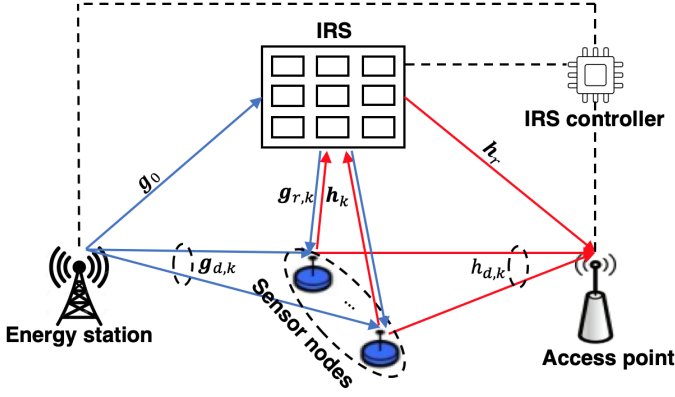


Fig. 1: An IRS assisted WPSN.

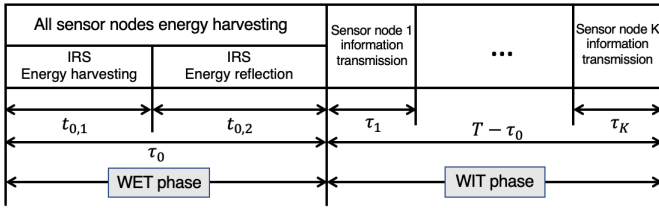


Fig. 2: IRS-HTT-TS transmission policy.

to the AP.¹ Coordinated by an IRS controller, the IRS supports passive energy/information beamforming to improve the energy/information transmission efficiency. The IRS requires a portion of energy consumption to support its own circuit operation. To schedule the transmission time slots, a whole operation time block is set to T , which can be split into two time periods, WET phase and WIT phase. During the WET phase, the IRS collects a portion of energy to support its own circuit operation and reflects the rest to improve energy reception of the sensor nodes. During the WIT phase, all sensor nodes utilize the harvested energy to deliver their own information to the AP with the IRS's help and in TDMA mode.² We denote τ_0 as the time duration for the WET phase, and $\tau_k, \forall k \in [1, K]$ as the time duration for the k -th sensor nodes during the WIT phase, all of which satisfies $\sum_{k=0}^K \tau_k = T$. To schedule the transmission time slots of WET phase, we adopt a time switching mode, where the first sub-slot is considered for the energy harvesting mode to support the circuit energy consumption of the IRS, and the second sub-slot is for the energy reflection mode to improve energy harvesting at the sensor nodes. This proposed novel transmission policy,

¹Although the work in [40] considered a similar system model, it integrated the information receiving station (i.e., AP) and the ES into one hybrid AP (HAP), which results in a lower hardware complexity but induces the doubly near-far issue [41]. In [40], the authors employed the *well-known* methods, such as one-dimensional line search and SDP relaxation, to numerically design the second sub-slot of the WET phase as well as jointly optimize the transmission time scheduling of the WIT phase and the phase shifts of the WET phase, respectively. In our work, a different modelling and a novel scheme are proposed, and in the following sections, we will highlight the advantages of our work by showing how it can effectively reduce the computational complexity.

²By setting the corresponding biasing voltages of the IRS varactors or PIN diodes or changing the value of resistors in each element, we can achieve the controllable reflection coefficients, i.e., phase shift and reflection amplitude, in every time slot of TDMA [18].

named, IRS-HTT-TS is illustrated in Fig. 2. In what follows, we focus on developing the suitable optimization strategies for the proposed transmission policy, and we are interested in the upper bounds of the sum throughput performance of different strategies for the considered system model. Therefore, perfect channel state information (CSI) is assumed in this work. Note that several channel estimation techniques have been investigated for the WPSN in the literature for obtaining the CSI of the direct link between ES and devices as well as that between devices and AP [41], [42]. One can also consider the passive pilots used for the channel estimation of the cascaded CSI. In particular, the reflecting elements of the IRS passively reflect the pilot sequences transmitted from the IoT devices to the AP/ES to the IoT devices such that the CSI associated with the IRS can be obtained [43]. On the other hand, the imperfect CSI cases have been investigated in [44]–[46], showing that the uncertainty of CSI or channel estimation errors can degrade system throughput. These imperfections can be tackled by using robust resource allocations for active transmit and passive reflecting beamformers [44]–[46]. To be specific, these robust schemes take into account the imperfect cascaded BS-IRS-user channels, which typically follow bounded and statistical CSI uncertainty, and the worst-case as well as outage probability robust beamforming designs are characterized. In addition, the channel coefficients between the ES and the k -th IoT device, the ES and the IRS, the IRS and the k -th IoT device, the k -th IoT device and the AP, the k -th IoT device and the IRS, as well as the IRS and the AP are denoted by $g_{d,k} \in \mathbb{C}^{1 \times 1}$, $\mathbf{g}_0 \in \mathbb{C}^{1 \times N_R}$, $\mathbf{g}_{r,k} \in \mathbb{C}^{N_R \times 1}$, $h_{d,k} \in \mathbb{C}^{1 \times 1}$, $\mathbf{h}_k \in \mathbb{C}^{1 \times N_R}$, and $\mathbf{h}_r \in \mathbb{C}^{N_R \times 1}$, respectively. We assume that all channels are quasi-static flat fading, and stay constant during one time block but may vary from one to another. Also, the perfect CSI for all transmission links are available to evaluate the upper bound for the system throughput.

A. Phase Shift Description

For the IRS, we denote $\Theta_k = \text{diag}[\beta_{k,1} \exp(j\alpha_{k,1}), \dots, \beta_{k,N} \exp(j\alpha_{k,N_R})], \forall k \in [0, K], n \in [1, N_R]$ as the diagonal phase shift matrix for different time durations, where $\alpha_{k,n} \in [0, 2\pi)$ and $\beta_{k,n} \in [0, 1]$ are the phase shift and reflection coefficient of the associated IRS reflecting elements, respectively. The phase shift of each reflecting element satisfies $|\exp(j\alpha_{k,n})| = 1$. When $k = 0$, Θ_0 is also known as the energy reflection phase shift matrix, whereas Θ_k is called the information reflection phase matrix when $k \in [1, K]$. Since the IRS is deployed to participate in the WET and WIT, aiming to maximize the energy and information reflection, the reflecting amplitude of each elements on the IRS should be set to a value of $\beta_{k,n} = 1, k \in [0, K], n \in [1, N_R]$ to achieve the maximum reflection gain. In practice, the phase shift of each element is designed to be finite number of discrete values, which can uniformly quantize the set of interval $[0, 2\pi)$ [47], i.e.,

$$\mathcal{S}_\Theta = \left\{ \theta_{k,n} = \exp(j\alpha_{k,n}), \alpha_{k,n} \in \left\{ 0, \frac{2\pi}{L}, \dots, \frac{2\pi(L-1)}{L} \right\} \right\}, \quad \forall k \in [0, K], \forall n \in [1, N_R], \quad (1)$$

where \mathcal{S}_Θ denotes the set of finite phase shifts, $L = 2^B$ is the total number of phase shift levels, and B denotes the number of bits used to indicate the number of phase resolutions.

B. Signal Processing of IRS-HTT-TS

Here, we describe the IRS-HTT-TS transmission policy from the signal processing perspective.

1) *Wireless Energy Transfer of IRS-HTT-TS Transmission Policy*: As shown in the left part of Fig. 2, the whole WET time slot is denoted by τ_0 , which can be split into two sub-slots, $t_{0,1}$ and $t_{0,2}$, and $\sum_{i=1}^2 t_{0,i} \leq \tau_0$. The sensor nodes collect wireless energy from the ES over the whole WET time slot. Also, the IRS harvests energy from the ES during the first sub-slot $t_{0,1}$ for its own circuit operation, and then it reflects energy from the ES to the sensor nodes during the second sub-slot $t_{0,2}$ to strengthen the energy reception at the sensor nodes. Thus, the received signals at the IRS during $t_{0,1}$, as well as at the k -th sensor node during $t_{0,1}$ and $t_{0,2}$, respectively, are given by

$$\begin{aligned} \mathbf{y}_r^{\text{TS}} &= \sqrt{P_0} \mathbf{g}_0^H x_0 + \mathbf{n}_{\text{IRS}}, \\ y_{k,i}^{\text{TS}} &= \begin{cases} \sqrt{P_0} g_{d,k} x_0 + n_k, & \text{During } t_{0,1}, \\ \sqrt{P_0} (\mathbf{g}_0 \Theta_0 \mathbf{g}_{r,k} + g_{d,k}) x_0 + n_k, & \text{During } t_{0,2}, \end{cases} \forall k \in [1, K], \end{aligned}$$

where x_0 denotes the energy signal with unit power, i.e., $x_0 \in \mathcal{CN}(0, 1)$, at the ES; P_0 denotes the transmit power at the ES; n_k and \mathbf{n}_{IRS} are the additive whit Gaussian noises at the k -th sensor node and the IRS, respectively.³ Accordingly, the energy collected by the IRS during $t_{0,1}$ and by the k -th sensor node during $t_{0,1}$ and $t_{0,2}$, respectively, can be represented by $E_{\text{TS,IRS}} = t_{0,1} \eta P_0 \|\mathbf{g}_0\|^2$, and $E_{\text{TS},k} = t_{0,1} \eta P_0 |g_{d,k}|^2 + t_{0,2} \eta P_0 |\mathbf{g}_0 \Theta_0 \mathbf{g}_{r,k} + g_{d,k}|^2$, $\forall k \in [1, K]$, where η denotes the energy harvesting efficiency.

2) *Wireless Information Transfer of IRS-HTT-TS*: During the WIT phase, all sensor nodes use the harvested energy to transmit their own message to the AP under the TDMA protocol, with the assistance of the IRS. Let P_k , $P_{c,k}$ and $P_{c,\text{IRS}}$ denote the transmit power, the circuit power consumption at the k -th sensor node, and the circuit power consumption at the IRS, respectively. In this paper, we consider the energy harvesting at the IRS to support its own circuit operation and at the IoT sensors to support their individual information transmission as well as circuit operation. For these purpose, two different relations are considered between the harvested energy and the required energy. To be specific, for the IRS, it follows the fact that the total energy consumption to support the IRS circuit operation during the second sub-slot of the WET phase and the whole WIT phase cannot exceed the harvested energy during the first sub-slot of the WET phase. For the IoT sensors, the harvested energy is consumed by each IoT sensor not only for supporting its information transmission, but also for supporting its circuit operation. Thus, the energy constraint on the k -th sensor is

$$\tau_k (P_k + P_{c,k}) \leq E_{\text{TS},k}, \quad \forall k \in [1, K]. \quad (2)$$

³Note that the noise power of the WET phase is typically ignored due to its negligible impact on energy harvesting. It is assumed based on the fact that the transmit power at the ES P_0 is sufficiently large [11].

To achieve self-sustainability, it should be guaranteed that the total energy consumption of the IRS's circuit operation does not exceed its harvested energy. Hence, the corresponding constraint can be written as

$$N_R P_{c,\text{IRS}} \left(t_{0,2} + \sum_{k=1}^K \tau_k \right) \leq E_{\text{TS,IRS}}. \quad (3)$$

In addition, the received signal from the k -th sensor node at the AP is given by

$$y_{\text{AP},k} = \sqrt{P_k} (\mathbf{h}_k \Theta_k \mathbf{h}_r + h_{d,k}) x_k + n_{\text{AP}}, \quad (4)$$

where $x_k \sim \mathcal{CN}(0, 1)$ denotes the information signal sent by the k -th sensor node; $n_{\text{AP}} \sim \mathcal{CN}(0, \sigma^2)$ denotes the AWGN at the AP. Thus, the achievable throughput of the k -th sensor node at the AP can be calculated as

$$R_k = \tau_k \log \left(1 + \frac{P_k |\mathbf{h}_k \Theta_k \mathbf{h}_r + h_{d,k}|^2}{\sigma^2} \right) \quad (5)$$

C. Problem formulation

To evaluate the IRS-HTT-TS transmission policy, we aim to maximize the achievable sum throughput, with a joint design of the phase shifts of the WET and WIT phases, the transmission time scheduling, as well as the transmit power allocation of all sensor nodes. The formulated problem is given as

$$\max_{\Omega_{\text{IRS-HTT-TS}}} \sum_{k=1}^K \tau_k \log \left(1 + \frac{P_k |\mathbf{h}_k \Theta_k \mathbf{h}_r + h_{d,k}|^2}{\sigma^2} \right), \quad (6a)$$

$$s.t. \quad (2), (3) \quad (6b)$$

$$\theta_{k,n} \in \mathcal{S}_\Theta, \quad \forall k \in [0, K], \quad \forall n \in [1, N_R], \quad (6c)$$

$$\sum_{i=1}^2 t_{0,i} \leq \tau_0, \quad (6d)$$

$$\sum_{k=0}^K \tau_k \leq T, \quad (6e)$$

$$t_{0,i} \geq 0, \quad \forall i \in [1, 2], \quad \tau_k \geq 0, \quad \forall k \in [0, K], \quad P_k \geq 0, \quad \forall k \in [1, K], \quad (6f)$$

where $\Omega_{\text{IRS-HTT-TS}} = \left[\{\Theta_k\}_0^K, \{t_{0,i}\}_1^2, \{\tau_k\}_0^K, \{P_k\}_1^K \right]$ assembles all variables of problem (6). In problem (6), (2) denotes the transmit power constraint of the k -th sensor node for the IRS-HTT-TS policy; (3) is the IRS power constraints for these policies; constraint (6c) denotes the discrete phase shift constraint; (6d) is the constraint of time scheduling during the WET; Constraint (6e) denotes the total time constraint; (6f) lists individual transmission time and power constraints. In our system model, the AP is typically equipped with multiple antennas, which employs the receive beamforming to decode the information received from different IoT sensors, instead of using TDMA. The associated problem formulation is given as (7) on the top of next page, where $\Omega_{\text{IRS-HTT-TS}} = \left[\{\Theta_0, \Theta_1\}, \{t_{0,i}\}_1^2, \{\tau_0, \tau_1\}, \{P_k\}_1^K \right]$ assembles all the variables of problem (7), $\mathbf{H}_r \in \mathbb{C}^{M \times N_R}$, $\mathbf{h}_k \in \mathbb{C}^{N_R \times 1}$, and $\mathbf{h}_{d,k} \in \mathbb{C}^{N_R \times 1}$. Note that problem (7) considers that the AP is equipped with M antennas such that TDMA is not necessary due to the receive beamformer \mathbf{w}_k , $\forall k \in [1, K]$ for the WIT

$$\begin{aligned}
& \max_{\Omega_{\text{IRS-HTT-TS}}} \sum_{k=1}^K \tau_1 \log \left(1 + \frac{P_k |\mathbf{w}_k (\mathbf{H}_r \Theta_1 \mathbf{h}_k + \mathbf{h}_{d,k})|^2}{\mathbf{w}_k \left[\sum_{j \neq k} P_j (\mathbf{H}_r \Theta_1 \mathbf{h}_j + \mathbf{h}_{d,j}) (\mathbf{H}_r \Theta_1 \mathbf{h}_j + \mathbf{h}_{d,j})^H + \sigma^2 \mathbf{I} \right] \mathbf{w}_k^H} \right), \\
& \text{s.t. } \sum_{i=1}^2 t_{0,i} \leq \tau_0, \quad \sum_{k=0}^1 \tau_k \leq T, \quad t_{0,i} \geq 0, \quad \forall i \in [1, 2], \quad \tau_k \geq 0, \quad \forall k \in [0, 1], \quad P_k \geq 0, \quad \forall k \in [1, K], \\
& |\exp(j\alpha_{k,n})| = 1, \quad \alpha_{k,n} \in [0, 2\pi), \quad \forall k \in [0, K], \quad \forall n \in [1, N_R], \\
& \tau_1 (P_k + P_{c,k}) \leq t_{0,1} \eta P_0 |g_{d,k}|^2 + t_{0,2} \eta P_0 |\mathbf{g}_0 \Theta_0 \mathbf{g}_{r,k} + g_{d,k}|^2, \quad \forall k \in [1, K], \\
& N_R P_{c,\text{IRS}} (t_{0,2} + \tau_1) \leq t_{0,1} \eta P_0 \|\mathbf{g}_0\|^2, \tag{7}
\end{aligned}$$

phase. This formulated problem includes multiple coupled received beamformer \mathbf{w}_k and phase shifts Θ_i , $\forall i \in [0, 1]$, which is not convex and cannot be solved directly. A possible solution is to employ the AO algorithm to alternately design \mathbf{w}_k and Θ_i [20]. Also, it is not possible to derive the optimal transmission time scheduling and phase shifts of the WET phase in closed-form. This because to achieve these, a more complicated derivation and reformulation have to be considered. However, for this scenario, it deserves another investigation, which is left for our future work.

III. ACHIEVABLE SUM THROUGHPUT MAXIMIZATION FOR IRS-HTT-TS

Problem (6) is not jointly convex due to multiple coupled variables in its objective function (6a) and constraint (2). Also, the phase shifts $\alpha_{k,n}$, $\forall k \in [0, K]$, $\forall n \in [1, N_R]$ in constraint (1) imply that (6) is a mixed-integer non-linear program (MINLP), which is typically NP-hard and cannot be solved directly. To deal with this issue, we first relax each discrete phase shift $\alpha_{k,n}$ to its continuous counterpart, i.e., $|\exp(j\alpha_{k,n})| = 1$, $\alpha_{k,n} \in [0, 2\pi)$, $\forall k \in [0, K]$, $\forall n \in [1, N_R]$. Thus, problem (6) is relaxed as

$$\max_{\Omega_{\text{IRS-HTT-TS}}} \sum_{k=1}^K \tau_k \log \left(1 + \frac{P_k |\mathbf{h}_k \Theta_k \mathbf{h}_r + h_{d,k}|^2}{\sigma^2} \right), \tag{8a}$$

$$\text{s.t. (2), (3), (6d), (6e), (6f),} \tag{8b}$$

$$|\exp(j\alpha_{k,n})| = 1, \quad \alpha_{k,n} \in [0, 2\pi), \quad \forall k \in [0, K], \quad \forall n \in [1, N_R]. \tag{8c}$$

Problem (8) is still non-convex with the multiple coupled variables. To circumvent this non-convexity, in the following, we will propose a two-step approach to solve it, where problem (8) is divided into two sub-problems, which can be separately solved.

A. Optimal Phase Shifts of WIT

In this subsection, we solve the first sub-problem with respect to the phase shifts of the WIT phase, i.e., Θ_k , $\forall k \in [1, K]$. To proceed, the following *theorem* is in order.

Theorem 1: The optimal phase shifts of the WIT phase, i.e., Θ_k , $\forall k \in [1, K]$ can be derived as

$$\Theta_k^* = \text{diag}(\theta_{k,1}^*, \dots, \theta_{k,N_R}^*), \quad \forall k \in [1, K], \quad \forall n \in [1, N_R], \tag{9}$$

where $\theta_{k,n}^* = \exp(j\alpha_{k,n}^*)$, $\alpha_{k,n}^* = \arg(h_{d,k}) - \arg(\mathbf{b}_k[n])$, and $\mathbf{b}_k = \text{diag}(\mathbf{h}_k) \mathbf{h}_r$.

Proof: See Appendix A. ■

Consequently, the following *lemma* is presented to clarify the impact of the optimal phase shifts, i.e., Θ_k on the signal reception enhancement at the AP.

Lemma 1: The optimal phase shifts of the WIT phase provide an alignment of the reflecting link between the sensor nodes and the AP via the IRS with the direct link between them, leading to the following relation

$$\mathbf{h}_k \Theta_k^* \mathbf{h}_r = \omega_k h_{d,k}, \quad \forall k \in [1, K], \tag{10}$$

where ω_k is positive scalar.

Proof: See Appendix B. ■

By exploiting *Lemma 1*, with the help of the IRS during the WIT phase, the signal reception of the k -th sensor node at the AP can be strengthened at most $(1 + \omega_k)^2$ times in comparison to the case without IRS [40]. Actually, ω_k , $\forall k \in [1, K]$ is proportionate to the reflecting elements of the IRS. Hence, more significant enhancement is introduced in terms of the sum throughput performance with a larger number of reflecting elements. Moreover, the IRS deployment as well as the path loss model of the reflecting link also significantly affect the signal reception at the AP [48].

After obtaining the optimal phase shifts of the WIT phase, we further solve problem (8) to optimally design the phase shift of the WET phase, the transmission time allocation, the transmit power of the sensor nodes. Denoting $c_k = |\mathbf{h}_k \Theta_k^* \mathbf{h}_r + h_{d,k}|^2$, we have

$$\max_{\Omega_{\text{IRS-HTT-TS}}} \sum_{k=1}^K \tau_k \log \left(1 + \frac{P_k c_k}{\sigma^2} \right), \tag{11a}$$

$$\text{s.t. (2), (3), (6d), (6e),} \tag{11b}$$

$$|\exp(j\alpha_{0,n})| = 1, \quad \alpha_{0,n} \in [0, 2\pi), \quad \forall n \in [1, N_R], \tag{11c}$$

$$t_{0,i} \geq 0, \quad \forall i \in [1, 2], \quad \tau_k \geq 0, \quad \forall k \in [0, K],$$

$$P_k \geq 0, \quad \forall k \in [1, K], \tag{11d}$$

$$\Omega_{\text{IRS-HTT-TS}} = \left[\Theta_0, \{t_{0,i}\}_1^2, \{\tau_k\}_0^K, \{P_k\}_1^K \right]. \tag{11e}$$

B. Optimal Solution to Problem (11)

In this subsection, we analyze the throughput performance of the proposed IRS-HTT-TS transmission policy via solving problem (11). To proceed, we begin with the special case (i.e., $P_{c,k} = 0$) and then the general case (i.e., $P_{c,k} \neq 0$).

1) *Special Case* ($P_{c,k} = 0$): Here, we consider the special case when the circuit power consumption of the k -th sensor

node equals to zero, i.e., $P_{c,k} = 0$.⁴ Thus, problem (11) is simplified to

$$\max_{\Omega_{\text{IRS-HTT-TS}}} \sum_{k=1}^K \tau_k \log \left(1 + \frac{P_k c_k}{\sigma^2} \right), \quad (12a)$$

$$s.t. \tau_k P_k \leq E_{\text{TS},k}, \quad (12b)$$

$$(3), (6d), (6e), (11c), (11d), (11e). \quad (12c)$$

Problem (12) is still non-convex and intractable. To solve it, we first consider the following *lemma* to handle the transmit power of the sensor nodes as well the sub-slots of the WET phase.

Lemma 2: The optimal transmit power of the k -th sensor node P_k^* , $\forall k \in [1, K]$ and the optimal second sub-slot of the WET phase $t_{0,2}^*$ should satisfy the following equalities:

$$P_k^* = \frac{t_{0,1}^* \eta P_0 |g_{d,k}|^2 + t_{0,2}^* \eta P_0 |\mathbf{g}_0 \Theta_0^* \mathbf{g}_{r,k} + g_{d,k}|^2}{\tau_k^*}, \quad (13a)$$

$$t_{0,2}^* = T - \sum_{k=1}^K \tau_k^* - t_{0,1}^*, \quad (13b)$$

where $t_{0,i}^*$, $\forall i \in [1, 2]$, τ_k , $\forall k \in [1, K]$, and Θ_0^* denote the optimal solutions of $t_{0,i}$, τ_k , and Θ_0 , respectively. In addition, the optimal first sub-slots of the WET phase $t_{0,1}^*$ can be derived in closed-form, as

$$t_{0,1}^* = \frac{N_R P_{c,\text{IRS}} T}{N_R P_{c,\text{IRS}} + \eta P_0 \|\mathbf{g}_0\|^2} \quad (14)$$

Proof: See Appendix C. ■

By applying *Lemma 2*, and defining $\tilde{c}_k = \frac{c_k \eta P_0}{\sigma^2}$, $\bar{c}_k = t_{0,1}^* |g_{d,k}|^2$ as well as $s_k = |\mathbf{g}_0 \Theta_0 \mathbf{g}_{r,k} + g_{d,k}|^2$, problem (12) can be further reformulated as

$$\max_{\Theta_0, t_{0,2}, \{\tau_k\}_1^K} \sum_{k=1}^K \tau_k \log \left(1 + \frac{\tilde{c}_k (\bar{c}_k + t_{0,2} s_k)}{\tau_k} \right), \quad s.t. (11c),$$

$$t_{0,2} \leq T - \sum_{k=1}^K \tau_k - t_{0,1}^*, \quad (15a)$$

$$t_{0,2} \geq 0, \tau_k \geq 0, \forall k \in [1, K], \quad (15b)$$

Problem (15) can be relaxed into a semidefinite programming (SDP), and solved directly by employing interior-point methods [49]. However, the SDP relaxation may incur a higher rank of the SDP based solution such that the Gaussian randomization technique should be adopted to construct an approximated feasible solution. This may introduce a high computational complexity and is time-consuming. It is thus imperative to develop a low complexity scheme which derives an optimal closed-form solution of the transmission time (i.e., $t_{0,2}$, and τ_k , $\forall k \in [1, K]$), as well as the phase shift of the WET phase (i.e., Θ_0). In order to perform the low complexity scheme, we first derive the transmission time of the WIT phase, i.e., τ_k , $\forall k \in [1, K]$, for which the following *theorem* is required,

Theorem 2: The optimal transmission time of the WIT

phase, i.e., τ_k , $\forall k \in [1, K]$, is derived in closed-form, as

$$\tau_k^* = \frac{(T - t_{0,1}^* - t_{0,2}) \tilde{c}_k (\bar{c}_k + t_{0,2} s_k)}{\sum_{k=1}^K \tilde{c}_k (\bar{c}_k + t_{0,2} s_k)} \quad (16)$$

Proof: See Appendix D. ■

We further substitute (16) in *Theorem 2* into (15), and define $\tilde{T} = T - t_{0,1}^*$, $c = \sum_{k=1}^K \tilde{c}_k \bar{c}_k$, as well as $s = \sum_{k=1}^K \tilde{c}_k s_k$, then (15) is equivalent to

$$\max_{t_{0,2}, \Theta_0} (\tilde{T} - t_{0,2}) \log \left(1 + \frac{c + t_{0,2} s}{\tilde{T} - t_{0,2}} \right) \quad (17a)$$

$$s.t. 0 \leq t_{0,2} < T, (11c) \quad (17b)$$

Problem (17) includes two variables, i.e., $t_{0,2}$ and Θ_0 , which can be optimally derived with the closed-form expressions. To solve (17), we first fix $t_{0,2}$ to derive the optimal closed-form solution of Θ_0 . Similar to *Theorem 1*, the maximization of (17) with respect to Θ_0 is equivalent to maximize the following problem

$$\max_{\Theta_0} \sum_{k=1}^K \tilde{c}_k |\mathbf{g}_0 \Theta_0 \mathbf{g}_{r,k} + g_{d,k}|^2, \quad s.t. (11c). \quad (18)$$

With some mathematical manipulations in the objective function of (18), we have

$$\sum_{k=1}^K \tilde{c}_k |\mathbf{g}_0 \Theta_0 \mathbf{g}_{r,k} + g_{d,k}|^2 = \sum_{k=1}^K \tilde{c}_k |\boldsymbol{\theta}_0 \mathbf{a}_k + g_{d,k}|^2, \quad (19)$$

where $\boldsymbol{\theta}_0 = [\exp(j\alpha_{0,1}), \dots, \exp(j\alpha_{0,N_R})]$, and $\mathbf{a}_k = \text{diag}(\mathbf{g}_0) \mathbf{g}_{r,k}$. Thus, (18) is equivalent to

$$\max_{\boldsymbol{\theta}_0} \sum_{k=1}^K \tilde{c}_k |\boldsymbol{\theta}_0 \mathbf{a}_k + g_{d,k}|^2$$

$$s.t. |\boldsymbol{\theta}_0(n)| = 1, \alpha_{0,n} \in [0, 2\pi], \forall n \in [1, N_R]. \quad (20)$$

To solve (20), we further expand its objective function as

$$\sum_{k=1}^K \tilde{c}_k |\boldsymbol{\theta}_0 \mathbf{a}_k + g_{d,k}|^2 = \boldsymbol{\theta}_0 \Phi_1 \boldsymbol{\theta}_0^H + 2\mathcal{R}\{\boldsymbol{\theta}_0 \boldsymbol{\gamma}\} + d_1. \quad (21)$$

where $\Phi_1 = \sum_{k=1}^K \tilde{c}_k \mathbf{a}_k \mathbf{a}_k^H$, $\boldsymbol{\gamma} = \sum_{k=1}^K \tilde{c}_k \text{conj}(g_{d,k}) \mathbf{a}_k$, $d_1 = \sum_{k=1}^K \tilde{c}_k |g_{d,k}|^2$. Substitute (21) into (20), we have

$$\min_{\boldsymbol{\theta}_0} \boldsymbol{\theta}_0 \Phi \boldsymbol{\theta}_0^H - 2\mathcal{R}\{\boldsymbol{\theta}_0 \boldsymbol{\gamma}\} + d \quad (22a)$$

$$s.t. |\boldsymbol{\theta}_0(n)| = 1, \forall n \in [1, N_R]. \quad (22b)$$

where $\Phi = -\Phi_1$ and $d = -d_1$. Problem (22) is still intractable due to its unit modulus equality constraint (22b). To solve (22), the MM algorithm is adopted to approximate its objective function and feasible set, which iteratively updates the approximated solution to (22) via an alternating algorithm [50]. To perform the MM algorithm, we first investigate the following problem

$$\min_{\mathbf{x}} f_0(\mathbf{x}), \quad s.t. f_i(\mathbf{x}) \leq 0, \quad x \in \mathcal{X}, \quad i = 1, \dots, L, \quad (23)$$

where $f_i(x) : \mathcal{X} \rightarrow \mathbb{R}$ denotes a continuous function, \mathcal{X} represents a non-empty closed set. We approximate both objective function and feasible constraints set of problem (23) at each iteration.⁵ Thus, the following convex sub-problem can

⁵Here we assume that f_i is differential [50].

⁴This case help us to obtain the upper bound of the achievable sum throughput for the proposed IRS-HTT-TS policy. A more general and practical case ($P_{c,k} \neq 0$) will be introduced in Section III-B2 that each sensor node collects energy to support its circuit operation during the WET.

be solved at the m -th iteration.

$$\min_{\mathbf{x}} g_0(\mathbf{x}|\mathbf{x}^{(m)}), \text{ s.t. } g_i(\mathbf{x}|\mathbf{x}^{(m)}) \leq 0, i = 1, \dots, L, \quad (24)$$

where $g_i(*|\mathbf{x}^{(m)})$, $\forall m = 0, \dots, L$ denotes a continuous surrogate function which guarantees the following conditions:

$$\begin{aligned} g_i(\mathbf{x}^{(m)}|\mathbf{x}^{(m)}) &= f_i(\mathbf{x}^{(m)}), \\ g_i(\mathbf{x}|\mathbf{x}^{(m)}) &\geq f_i(\mathbf{x}), \\ \nabla g_i(\mathbf{x}^{(m)}|\mathbf{x}^{(m)}) &= \nabla f_i(\mathbf{x}^{(m)}). \end{aligned} \quad (25)$$

From (25), it is easily observed that the sequence $\mathbf{x}^{(m)}$ obtained from (24) at each iteration leads to a monotonically decreasing function, i.e., $f_0(\mathbf{x}^{(m)})$, $m = 1, 2, \dots$ which converges to a KKT point [50]. The first and third conditions denote that the surrogate function $g_i(\mathbf{x}^{(m)}|\mathbf{x}^{(m)})$ and its first-order approximation are the same as the original function $f_i(\mathbf{x}^{(m)})$ and its first-order approximation at $\mathbf{x}^{(m)}$. The second condition implies that the surrogate function $g_i(\mathbf{x}|\mathbf{x}^{(m)})$ is constructed based on the upper bound of the original function $f_i(\mathbf{x}^{(m)})$. To perform the MM algorithm, it is imperative to achieve the surrogate function $g_i(\mathbf{x}|\mathbf{x}^{(m)})$, guaranteeing these conditions (25) and better tractability than $f_i(\mathbf{x}^{(m)})$ [25], [50].

The following *theorem* is required to derive the optimal closed-form solution of θ_0 by the MM algorithm.

Theorem 3: The optimal solution to problem (22) is derived in terms of the following closed-form expression via the MM algorithm.

$$\theta_0^* = \left[\exp(j \arg[\tilde{\gamma}(1)]) , \dots, \exp(j \arg[\tilde{\gamma}(N_R)]) \right], \quad (26)$$

where $\tilde{\gamma} = (\lambda_{\max}(\Phi) \mathbf{I}_{N_R \times N_R} - \Phi) \tilde{\theta}_0^H + \gamma$; $\lambda_{\max}(\Phi)$ is the maximum eigenvalue of Φ ; $\tilde{\theta}_0$ denotes the approximated solution to θ_0 which is achieved in the previous iteration of the alternating algorithm.

Proof: See Appendix E. ■

Remark 1: In (26), we obtain the optimal phase shift of the WET phase, which can be independently applied to the IRS to maximize the energy signal strength at sensor nodes. Although problem (20) can be easily relaxed as an SDP, (26) provides an optimal solution which is more efficient for implementation and significantly reduces the computational complexity introduced by the SDP, especially for the larger reflecting elements N_R .

Since the optimal solution of θ_0 can be iteratively updated via the approximation of the MM algorithm, its convergence property is characterized as follows. The MM algorithm shows that the objective value $f(\theta_0)$ is monotonically non-increasing at each iteration, i.e.,

$$f(\theta_0^{(m+1)}) \leq g(\theta_0^{(m+1)}|\theta_0^{(m)}) \leq g(\theta_0^{(m)}|\theta_0^{(m)}) = f(\theta_0^{(m)}), \quad (27)$$

where $\theta_0^{(m)}$ denotes the point generated by the MM algorithm at the m -th iteration. From (27), the first inequality and the third equality follow the first two relations of (25), respectively. Also the second inequality holds via solving

$$\theta_0^* = \arg \min_{\theta_0(n)} g(\theta_0|\tilde{\theta}_0), \text{ s.t. } |\theta_0(n)| = 1, \forall n \in [1, N_R]. \quad (28)$$

The monotonicity of the objective function in the above problem confirms that the MM algorithm converges to a stationary point in practice due to the unit modulus equality constraint [50], [51].

By exploiting *Theorem 3*, the optimal phase shift matrix of the WET, i.e., Θ_0^* , can be achieved from θ_0^* . For a given Θ_0^* , problem (17) is a single-variable optimization problem which can easily be proved to be convex with respect to $t_{0,2}$. Thus, it can be solved via one-dimensional line search, i.e., golden search method. Here, we derive the optimal second sub-slot of the WET phase in terms of closed-form expression via the following *theorem*:

Theorem 4: The optimal second sub-slot of the WET phase, i.e., $t_{0,2}^*$ is derived as

$$t_{0,2}^* = \frac{\left\{ \exp \left[\mathcal{W} \left(\frac{s-1}{\exp(1)} \right) + 1 \right] - 1 \right\} \tilde{T} - c}{s + \exp \left[\mathcal{W} \left(\frac{s-1}{\exp(1)} \right) + 1 \right] - 1}. \quad (29)$$

Proof: See Appendix F. ■

The proposed low complexity algorithm to solve problem (8) is summarized in *Algorithm 1*. Now, we characterize the computational complexity of *Algorithm 1*, which depends upon the proposed MM algorithm. Thus, the total computational complexity of the MM algorithm is given as $\mathcal{O}(N_R^3 + I_{\max} N_R^2)$, where I_{\max} is the number of iterations the MM algorithm to achieve convergence.

Algorithm 1: Proposed algorithm for the special case ($P_{c,k} = 0$) to solve problem (8).

- 1) **Input:** P_0 , η , and c_k , $\forall k \in [1, K]$.
 - 2) **Obtain** the optimal phase shifts of the WIT phase Θ_k , $\forall k \in [1, K]$ according to θ_k^* in (39).
 - 3) **Obtain** the first sub-slot of the WET phase $t_{0,1}^*$ via (14) in *Lemma 2*.
 - 4) **Obtain** the optimal phase shift of the WET phase Θ_0^* , which is from θ_0^* in (26) via the MM algorithm.
 - 5) **Obtain** the second sub-slot of the WET phase $t_{0,2}^*$ via (29) in *Theorem 4*.
 - 6) **Substitute** Θ^* and $t_{0,i}^*$, $\forall i \in [1, 2]$ into (16) to obtain the optimal time allocation of the WIT phase τ_k^* , $k \in [1, K]$.
 - 7) **Substitute** Θ^* , $t_{0,i}^*$, and τ_k into (13a) in *Lemma 2* to obtain the optimal transmit power of each IoT sensor P_k , $\forall k \in [1, K]$.
 - 8) **Output:** $t_{0,i}^*$, $\forall i \in [1, 2]$, τ_k^* , $\forall k \in [0, K]$, Θ_k^* , $\forall k \in [0, K]$, and P_k^* , $\forall k \in [1, K]$.
-

2) *General Case* ($P_{c,k} \neq 0$): In this subsection, we consider the general case of $P_{c,k} \neq 0$, which is more practical and complex than the special case studied in Section III-B1. Here, we write problem (8) as

$$\begin{aligned} \max_{\Omega_{\text{IRS-HTF-TS}}} \sum_{k=1}^K \tau_k \log \left(1 + \frac{P_k c_k}{\sigma^2} \right), \quad (30a) \\ \text{s.t. (2), (3), (6d), (6e), (11c), (11d), (11e), (30b)} \end{aligned}$$

Due to the non-convexity of problem (30), we introduce the SDP relaxation to solve it. To proceed, we define $\tilde{P}_k = \tau_k P_k$, $\mathbf{W}_0 = t_{0,2} \mathbf{V}_0$, $\mathbf{V}_0 = \tilde{\theta}_0^H \tilde{\theta}_0$, $\tilde{\theta}_0 = [\theta_0 \ 1]$, $\tilde{\mathbf{a}}_k = \begin{bmatrix} \mathbf{a}_k \\ g_{d,k} \end{bmatrix}$, $\mathbf{A}_k = \tilde{\mathbf{a}}_k \tilde{\mathbf{a}}_k^H$, and $\mathbf{a}_k = \text{diag}(\mathbf{g}_0) \mathbf{g}_{r,k}$ to handle the objective function (30a) and the constraint (2), respectively. In addition,

the optimal first sub-slot of the WET phase $t_{0,1}^*$ can be derived as (14) in *Lemma 2*. Thus, problem (30) is relaxed as

$$\max_{\Omega_{\text{IRS-HTT-TS}}} \sum_{k=1}^K \tau_k \log \left(1 + \frac{\tilde{P}_k c_k}{\tau_k \sigma^2} \right), \quad (31a)$$

$$s.t. \tilde{P}_k + \tau_k P_{c,k} \leq t_{0,1} \eta P_0 |g_{d,k}|^2 + \eta P_0 \text{Tr}(\mathbf{A}_k \mathbf{W}_0), \quad (31b)$$

$$N_R P_{c,\text{IRS}} \left(t_{0,2} + \sum_{k=1}^K \tau_k \right) \leq t_{0,1}^* \eta P_0 \|\mathbf{g}_0\|^2, \quad (31c)$$

$$t_{0,1}^* + t_{0,2} + \sum_{k=1}^K \tau_k \leq T, \quad (31d)$$

$$\mathbf{W}_0(n, n) = t_{0,2}, \quad \forall n \in [1, N_R + 1], \quad (31e)$$

$$\mathbf{W}_0 \succeq \mathbf{0}, \quad (31f)$$

$$\text{rank}(\mathbf{W}_0) = 1, \quad (31g)$$

$$t_{0,2} \geq 0, \quad \tau_k \geq 0, \quad \forall k \in [0, K], \quad (31h)$$

$$\tilde{P}_k \geq 0, \quad \forall k \in [1, K], \quad (31h)$$

$$\Omega_{\text{IRS-HTT-TS}} = \left[\mathbf{W}_0, t_{0,2}, \{\tau_k\}_1^K, \{\tilde{P}_k\}_1^K \right]. \quad (31i)$$

By relaxing the non-convex rank-one constraint (31g), it can be easily verified that (31) is a convex optimization problem, which can be solved by the interior-point methods [49]. The optimal solution of problem (31) is represented by $(\mathbf{W}_0^*, t_{0,2}^*, \{\tau_k^*\}_1^K, \{\tilde{P}_k^*\}_1^K)$, and we further obtain the optimal solution $\mathbf{V}_0^* = \frac{\mathbf{W}_0^*}{\tau_0^*}$ and $P_k = \frac{\tilde{P}_k^*}{\tau_k^*}$. Note that the relaxed problem (31) may incur a higher rank solution, i.e., $\text{rank}(\mathbf{V}_0^*) > 1$. To circumvent this issue, we apply eigenvalue decomposition on \mathbf{V}_0^* , yielding, $\mathbf{V}_0^* = \mathbf{\Upsilon} \mathbf{\Lambda} \mathbf{\Upsilon}^H$, where $\mathbf{\Upsilon} \in \mathbb{C}^{(N_R+1) \times (N_R+1)}$ is a unitary matrix, and $\mathbf{\Lambda} \in \mathbb{C}^{(N_R+1) \times (N_R+1)}$ is a diagonal matrix with eigenvalues arranged in decreasing order. To proceed, we construct a suboptimal solution as $\tilde{\theta}_0^H = \mathbf{\Upsilon} \mathbf{\Lambda}^{\frac{1}{2}} \boldsymbol{\kappa}$, where $\boldsymbol{\kappa} \in \mathbb{C}^{(N_R+1) \times 1}$ is randomly generated to follow complex circularly symmetric uncorrelated Gaussian distribution with zero-mean and covariance matrix $\mathbf{I}_{(N_R+1) \times (N_R+1)}$. Thus, we obtain the optimal phase shift vector $\theta_0^*(n) = \exp(j \arg(\tilde{\theta}_0(n)))$ for $n \in [1, N_R]$ and the optimal phase shift matrix Θ_0^* can be achieved from θ_0^* [20]. Since (30) can be relaxed to a convex problem that satisfies Slater's condition, the strong duality holds. To gain more insights, we characterize the optimal closed-form solution of the time allocation, i.e., $t_{0,i}$, $\forall i \in [1, 2]$ and τ_k , $\forall k \in [1, K]$ for given phase shifts Θ_k^* , $\forall k \in [0, K]$. Note that the optimal first sub-slot of the WET phase $t_{0,1}^*$ has been derived as (14) in *Lemma 2*. To proceed, we modify (30) to an equivalent form of

$$\max_{t_{0,2}, \tau_k} \sum_{k=1}^K \tau_k \log \left(1 + \frac{a_k + t_{0,2} b_k}{\tau_k} - d_k \right), \quad (32a)$$

$$s.t. t_{0,1}^* + t_{0,2} + \sum_{k=1}^K \tau_k \leq T, \quad (32b)$$

$$t_{0,2} \geq 0, \quad \tau_k \geq 0, \quad \forall k \in [1, K]. \quad (32c)$$

where $a_k = \bar{c}_k \tilde{c}_k$, $b_k = s_k^* \tilde{c}_k$, $d_k = P_{c,k} \hat{c}_k$, $\hat{c}_k = \frac{c_k}{\sigma^2}$, and $s_k^* = |\mathbf{g}_0 \Theta_0^* \mathbf{g}_{r,k} + g_{d,k}|^2$. To derive the optimal solution of problem (32), the following *theorem* is in order.

Theorem 5: The optimal closed-form time slots of problem

(32), e.g., $\tilde{t}_{0,2}^*$ and $\tilde{\tau}_k$, $\forall k \in [1, K]$, are derived, respectively, as

$$\tilde{t}_{0,2}^* = \frac{T - t_{0,1}^* - \sum_{k=1}^K \frac{a_k}{x_k^*}}{1 + \sum_{k=1}^K \frac{b_k}{x_k^*}}, \quad \tilde{\tau}_k^* = \frac{a_k + t_{0,2}^* b_k}{x_k^*}. \quad (33)$$

Proof: See Appendix G. \blacksquare

Theorem 5 unveils an insight that when the phase shifts of the WET and WIT stages are given, we can calculate the optimal time slots $t_{0,1}^*$, $\tilde{t}_{0,2}^*$, and $\tilde{\tau}_k^*$ to obtain the maximum achievable sum throughput.

C. Discrete Phase Shift Optimization

In Section III-A and Section III-B, we obtained the optimal continuous phase shifts for the WIT and WET phases. In this subsection, we obtain the quantized phase shifts according to constraint (1). We denote the optimal continuous phase shifts as $\theta^* = \{\theta_0^*, \dots, \theta_K^*\}$, where $\theta_k^* = [\theta_{k,1}^*, \dots, \theta_{k,N_R}^*]$, $\forall k \in [0, K]$ is derived in Section III-A and Section III-B, and substituted into (1). Thus, the optimal discrete phase shift of the n -element at the k -time slot, denoted by $\theta_{k,n}^*$ is derived as

$$\bar{\theta}_{k,n}^* = \exp(j\alpha l^*), \quad (34)$$

where $l^* \in [1, L]$ denotes the optimal index of discrete phase shift set \mathcal{S}_Θ , which can be determined by solving the following problem

$$l^* = \arg \min_{l \in [1, L]} \left| \bar{\theta}_{k,n}^* - \exp(j\alpha l) \right|. \quad (35)$$

Note that the discrete optimal phase shifts of the IRS can be obtained by first solving (8) with the continuous phase shifts instead of (6), and then quantizing the continuous phase shifts to their nearest points from \mathcal{S}_Θ via (34).

IV. NUMERICAL RESULTS

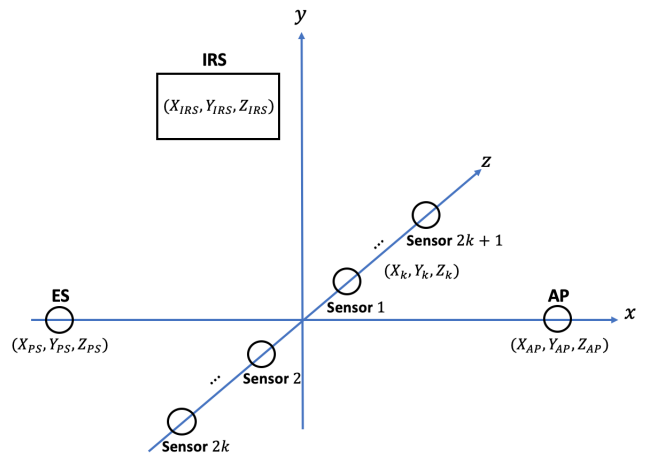


Fig. 3: System deployment.

This section provides numerical evaluations to validate the theoretical derivations of the proposed IRS-HTT-TS policy in Section III. In our simulations, we use a three-dimensional (3D) coordinate in Fig. 3 showing the possible deployment of the IRS assisted WPSN. Specifically, we assume that the

coordinates of the ES, the AP, and the IRS are located at $(-10, 0, 0)$, $(10, 0, 0)$ and $(-2, 6, 0)$, respectively, while the sensor nodes are assigned at $(0, 0, \frac{l \times d_I}{2})$ if $l = 1, \dots, (2k + 1)$, and $(0, 0, -\frac{(l-1) \times d_I}{2})$, if $l = 2, \dots, 2k$, where d_I is the separation distance between two neighbouring sensors. The channel coefficient is composed of distance-dependent path loss model and small-scale fading. The path loss model is set to $P_L = Ad^{-\varepsilon}$, where $A = -20$ dB, ε is the path loss exponent, and d represents the distance between any two devices, i.e., the ES and the IRS, the ES and the k -th sensor node, the IRS and the k -th sensor node, the IRS and the AP, as well as the k -th sensor node and the AP. The channel coefficients between the ES and the IRS, the IRS and the k -th sensor node, the k -th sensor node and the IRS, as well as the IRS and the AP are modelled as $\mathbf{g}_0 = \sqrt{\frac{K_1}{K_1+1}} \mathbf{g}_0^{\text{LOS}} + \sqrt{\frac{1}{K_1+1}} \mathbf{g}_0^{\text{NLOS}}$, $\mathbf{g}_{r,k} = \sqrt{\frac{K_1}{K_1+1}} \mathbf{g}_{r,k}^{\text{LOS}} + \sqrt{\frac{1}{K_1+1}} \mathbf{g}_{r,k}^{\text{NLOS}}$, $\mathbf{h}_k = \mathbf{g}_{r,k}^T$, and $\mathbf{h}_r = \sqrt{\frac{K_1}{K_1+1}} \mathbf{h}_r^{\text{LOS}} + \sqrt{\frac{1}{K_1+1}} \mathbf{h}_r^{\text{NLOS}}$. Specifically, $\mathbf{g}_0^{\text{LOS}}$, $\mathbf{g}_{r,k}^{\text{LOS}}$, and $\mathbf{h}_r^{\text{LOS}}$ denote the line-of-sight (LOS) deterministic components of the corresponding channel coefficients. Also, we denote one of the array responses as $\mathbf{g}_0^{\text{LOS}} = [1, \exp(-j\frac{2\pi d}{\lambda} \phi), \dots, \exp(-j\frac{2\pi(N_R-1)d}{\lambda} \phi)]$ and others are similarly generated, where λ denotes the carrier wavelength, $\phi = \cos^{-1}(\frac{X_{PS} - X_{IRS}}{d_{PS2IRS}})$ is the angle of arrival(AoA)/angle of departure(AoD); $\mathbf{g}_0^{\text{NLOS}}$, $\mathbf{g}_{r,k}^{\text{NLOS}}$, and $\mathbf{h}_r^{\text{NLOS}}$ are the non-line-of-sight (NLOS) components of the corresponding channel coefficients which follow the Rayleigh distribution; K_1 is the Rician factor which is set to 6 dB without loss of generality. The remaining small-scale channel coefficients are generated as circularly symmetric Gaussian random variables with zero mean and unit variance. Other configurations of the simulations are summarized as: the total transmission time period $T = 1$ s, number of the reflecting elements at the IRS $N_R = 30$, number of sensor nodes $K = 6$, transmit power at the ES $P_0 = 30$ dBm, noise power at the AP $\sigma^2 = -100$ dBm, energy conversion efficiency $\eta = 0.8$, the circuit power of the k -th sensor node as well as the IRS $P_{c,k} = P_{c,IRS} = P_c = 0.01$ mW. The selected configurations and parameters, especially those related to the power and energy, are widely considered in the literature, e.g., [52], and the low-power circuit has been justified and supported by the practical investigations, e.g., [53]. The number of bits used to indicate the number of phase resolution $B = 1$ or 2, respectively, unless specified. We evaluate the performance gains of the proposed low complexity scheme in comparison to the following benchmark schemes:

- 1) *SDP relaxation*: In the special case, problem (12) is relaxed as a convex optimization problem, and solved directly by interior-point methods [49].
- 2) *Random phase shift*: The phase shifts are randomly generated, whereas the transmission time slots are optimally designed in Section III-B.
- 3) *Without IRS*: This system model degrades into the conventional WPSN [11], where the transmission time allocations are optimally designed.
- 4) *Upper bound*: In this scheme, the IRS does not consider

the energy collection to support its circuit operation, i.e., $P_{c,IRS} = 0$, which leads to the first sub-slots of the WET phase $t_{0,1} = 0$.

To distinguish different schemes, “SDP” and “SDP: discrete phase shift ($B = 1$ or 2)” denote the SDP relaxation with continuous and discrete phase shifts, respectively; “LC” and “LC: discrete phase shift ($B = 1$ or 2)” denote the proposed low complexity scheme with continuous and discrete phase shifts, respectively.

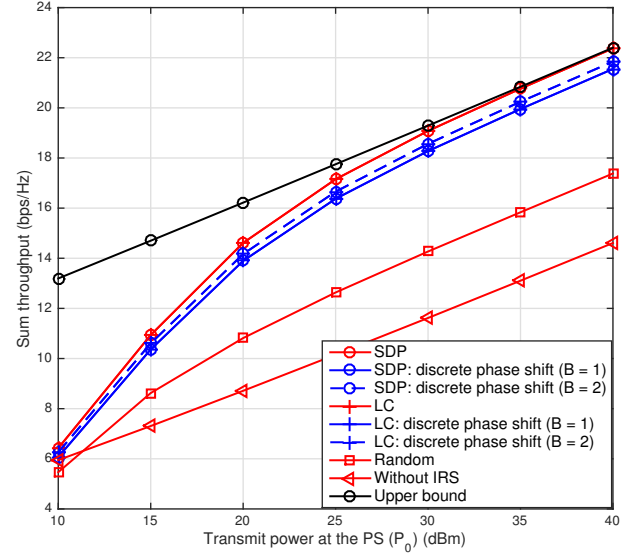


Fig. 4: Sum throughput versus transmit power at the ES P_0 for special case.

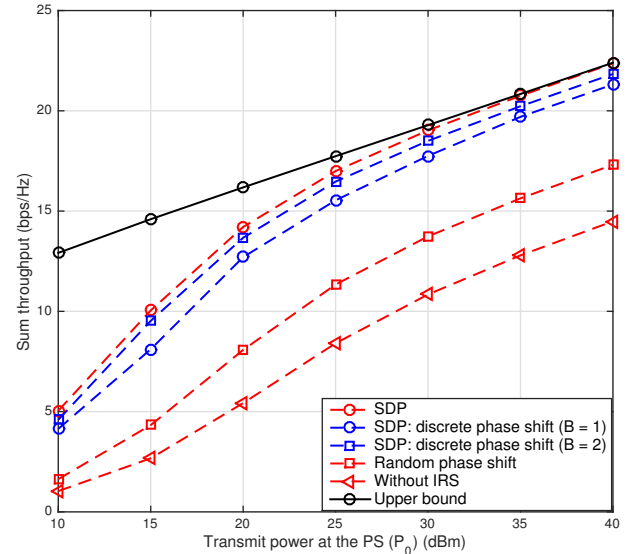


Fig. 5: Sum throughput versus transmit power at the ES P_0 for general case.

First, we evaluate the sum throughput versus the transmit power at the ES P_0 for the special and general cases in

Fig. 4 and Fig. 5. From these results, it is seen that the sum throughput has an increasing trend with P_0 . Also, the scheme with continuous phase shifts slightly outperforms its counterpart with quantized phase shifts $B = 1$ or 2. This is due to the fact that the quantized phase shifts leads to the imperfect alignment between the direct and reflected links for the WET and WIT phases and results in a performance loss. In addition, the quantized phase shift case with $B = 2$ has a slightly higher sum throughput than that with $B = 1$. This is due to the fact that a larger B brings higher granularity of phase shifts to be selected for energy/information reflection. Moreover, the proposed scheme has an obvious performance gain compared with the schemes with random phase shifts and without IRS, which demonstrates the beneficial role of IRS to enhance the WET and WIT, especially in the large transmit power region. From Fig. 4, one can also observe that the proposed low complexity scheme achieves a very close performance with the SDP relaxed counterpart, which verifies the effectiveness of our proposed low complexity scheme derived in Section III-B.

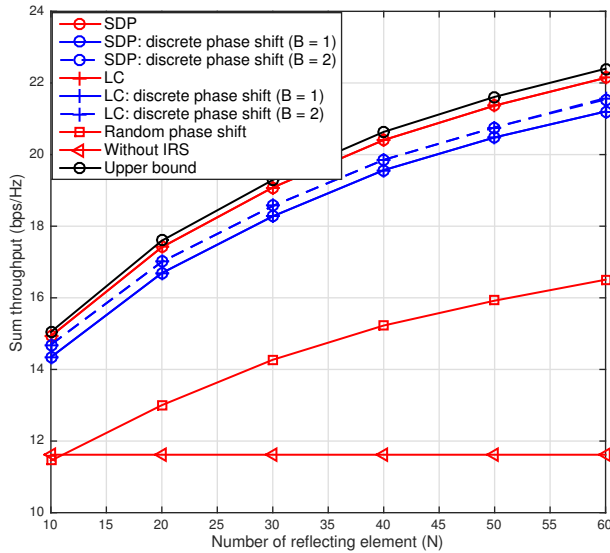


Fig. 6: Sum throughput versus number of reflecting elements N_R for special case.

Fig. 6 and Fig. 7 evaluate the impact of the number of reflecting elements N on the sum throughput. From these results, we see that the proposed scheme can effectively enhance the sum throughput with more reflecting elements in comparison to the schemes with random phase shift and without IRS. Also, the scheme with quantized phase shifts $B = 1$ or 2 has a slight performance loss than that with continuous phase shifts. This is because the quantized phase shifts incur imperfect alignment between the direct and reflected links for the WET and WIT phases, resulting in degraded throughput performance. To validate the proposed low complexity scheme, we compare it with the SDP relaxed scheme. By comparison, the two schemes have a comparable performance, which confirms the effectiveness of our proposed low complexity scheme derived

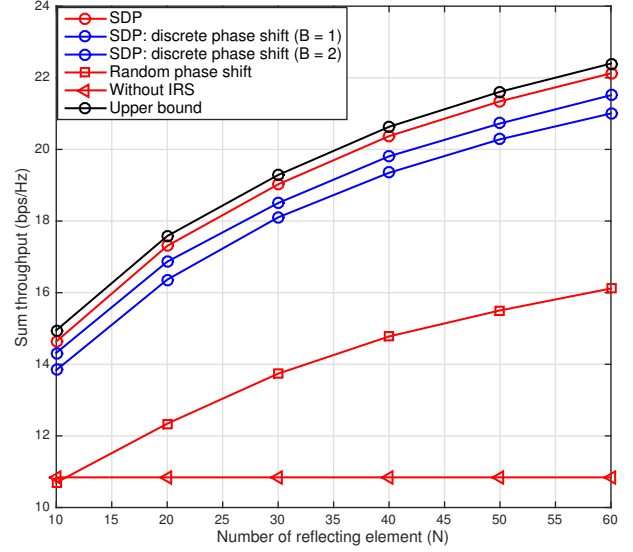


Fig. 7: Sum throughput versus number of reflecting elements N_R for general case.

in Section III-B.

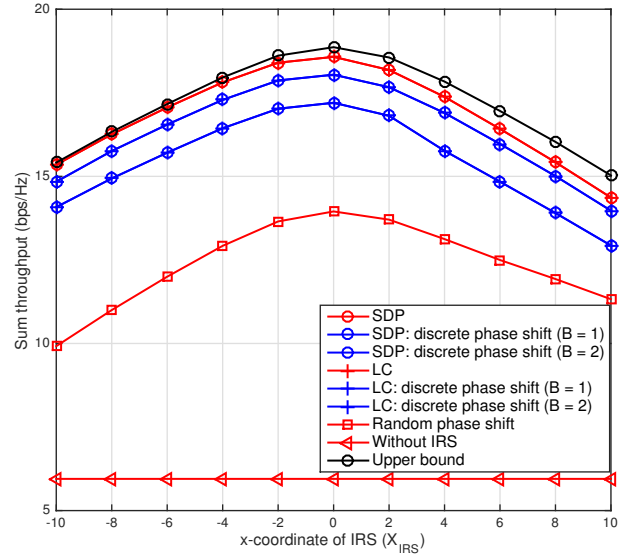


Fig. 8: Sum throughput versus x-coordinate of IRS X_{IRS} for special case.

Next, the impact of the IRS deployment on the sum throughput is illustrated for the special and general cases in Fig. 8 and Fig. 9, respectively. It is seen from these results that the sum throughput first increases and then declines with x-coordinate of the IRS X_{IRS} . This justifies the optimal deployment of the IRS to maximize the energy collection reception at the sensor nodes and the information reception at the AP, respectively. Also, the scheme with continuous phase shifts slightly outperforms its counterpart with discrete phase shifts, all of which have an obvious advantage over the

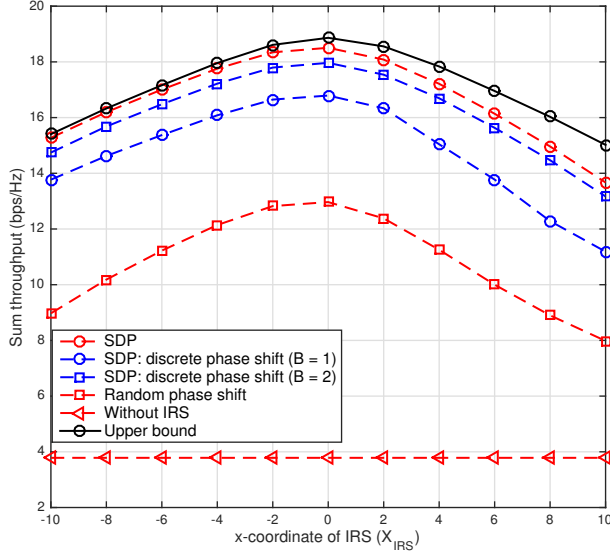


Fig. 9: Sum throughput versus x-coordinate of IRS X_{IRS} for general case.

schemes with random phase shifts and the one without IRS. In addition, a larger number of bits B yields a better performance, and the proposed low complexity scheme is closely matched with the SDP relaxed scheme.

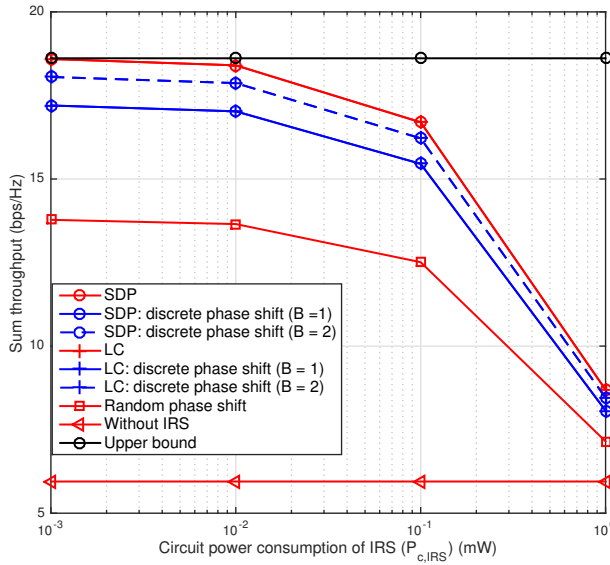


Fig. 10: Sum throughput versus circuit power consumption of IRS $P_{c,\text{IRS}}$ for special case.

We evaluate the sum throughput versus the circuit power consumption of the IRS $P_{c,\text{IRS}}$ for the special and general cases in Fig. 10 and Fig. 11, respectively. As $P_{c,\text{IRS}}$ increases, the sum throughput has an decreasing trend, which is more significant at the higher circuit power region. This unveils the fact that the IRS requires more energy to support its own circuit operation at the first sub-slot of the WET, thus cuts

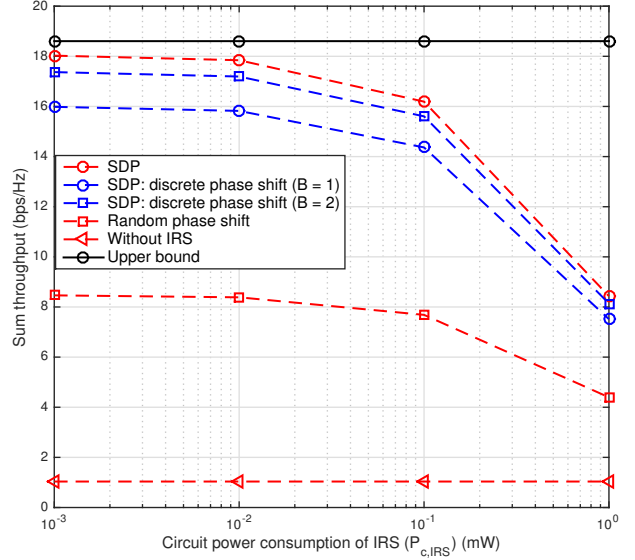


Fig. 11: Sum throughput versus circuit power consumption of IRS $P_{c,\text{IRS}}$ for general case.

down its energy reflection at the second sub-slot of the WET.

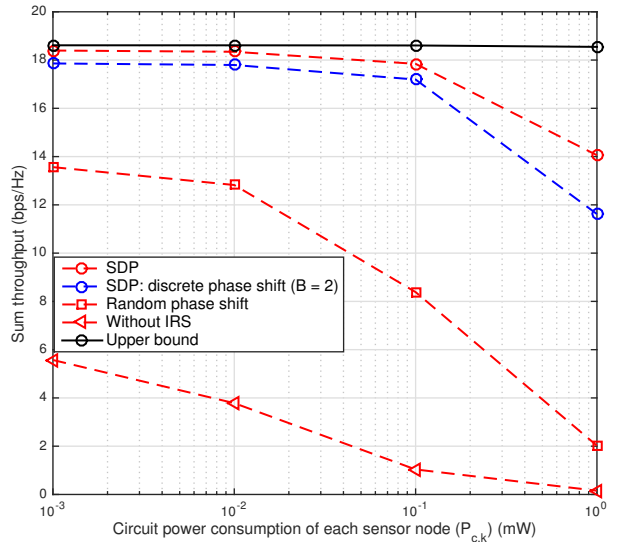


Fig. 12: Sum throughput versus circuit power consumption of sensor nodes $P_{c,k}$ for general case.

Moreover, we evaluate the impact of circuit power consumption of the sensor nodes $P_{c,k}$ on sum throughput for the general case in Fig. 12.⁶ From this result, we observe that the sum throughput decreases with $P_{c,k}$, which becomes more evident in the higher circuit power region. This reveals the fact that the sensor nodes require more energy to support its own circuit operation so as to cut down its portion of energy for the WIT.

⁶We do not need to evaluate the sum throughput versus the circuit power consumption of the sensor nodes $P_{c,k}$, since the special case is not affected by $P_{c,k}$.

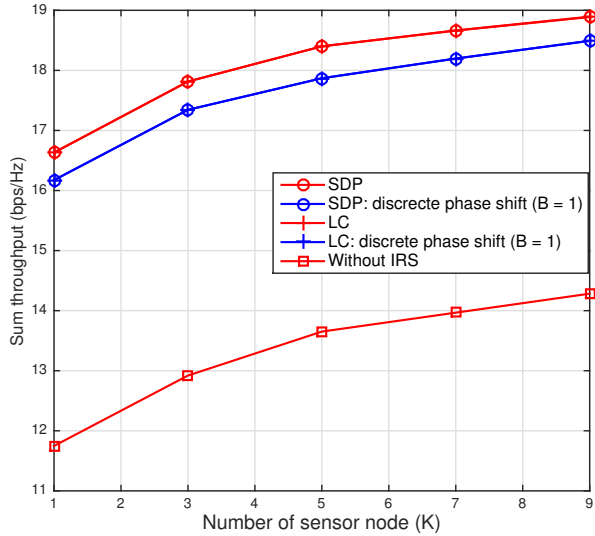


Fig. 13: Sum throughput versus number of sensor nodes (K).

Finally, the impact of the number of sensor nodes K on the sum throughput performance is illustrated in Fig. 13, where the sum throughput has an increasing relation with the number of sensor nodes K . It is also worth mentioning that, as K increases, more sensors are located farther away from the ES, the IRS, and the AP (refer to the system deployment in Fig. 3), which degrades the energy and information reflection efficiencies, resulting in that the throughput gain becomes smaller.

V. CONCLUSION

This studied an IRS assisted WPSN, where the IRS aims to harvest energy from an ES to support its circuit operations and reflect energy and information signals to enhance WET and WIT performance. We proposed a novel IRS-HTT-TS transmission policy to schedule the time slots during the WET phase. We are interested in maximizing the system sum throughput to design the discrete phase shifts of the WET and WIT stages, the power allocation of the sensors, and the transmission time scheduling. We first relaxed the original problem to the one with continuous phase shifts to deal with its NP-hard nature. To solve the relaxed non-convex problem, a two-step approach was proposed to decompose it into two sub-problems, which can be independently solved. The optimal closed-form phase shifts of the WIT stage were derived in closed-form. Furthermore, we specifically investigated two cases without/with the circuit power consumption of each sensor to optimally design the phase shift for the WET, the power allocation of each sensor as well as the transmission time scheduling. In addition, we considered the quantization of the continuous phase shifts to obtain the optimal discrete counterparts. Finally, the benefits of the proposed schemes were validated by numerical evaluations and shown to significantly enhance the sum throughput performance of the IRS assisted WPSN under study.

The proposed approach has established an analytical framework for further investigation on the IRS aided WPSN, where the system model, transmission protocol and performance analysis can serve as a benchmark for the cases, such as, the network considered in this paper but instead with a non-linear energy harvesting model, where novel fractional energy harvesting models can be considered in the joint design of the phase shifts of the WET and WIT phases. Correspondingly, an extended system model with a multi-antenna ES or AP, where the active energy or active receiving and passive reflecting beamformers, as well as the transmission time slots can be alternately optimized. In addition, the impact of channel estimation errors, pilot overhead and hardware impairments on the throughput performance may be introduced by leveraging channel estimation algorithm, which is considered as one of our future work. Specifically, robust design will be studied in the IRS assisted WPSN to cope with the imperfect channel estimation, where the direct and cascaded channel estimation errors can be modelled as deterministic or statistical quantities. Moreover, the IRS can be applied to mobile edge computing or wireless edge caching to improve the computational or wireless caching capabilities, which forges a novel paradigm for an integrated communication, sensing and computing network.

APPENDIX

A. Proof of Theorem 1

According to (5), it is readily verified that R_k is a monotonically increasing function in the term $|\mathbf{h}_k \Theta_k \mathbf{h}_r + h_{d,k}|^2$. Thus, the optimal solution of Θ_k is obtained by solving problem (8), which is equivalent to solving the following K sub-problem

$$\begin{aligned} \max_{\Theta_k} & |\mathbf{h}_k \Theta_k \mathbf{h}_r + h_{d,k}|^2, \quad s.t. \quad |\exp(j\alpha_{k,n})| = 1, \\ & \alpha_{k,n} \in [0, 2\pi), \quad \forall k \in [1, K], \quad \forall n \in [1, N_R]. \end{aligned} \quad (36)$$

Problem (36) only relies on Θ_k with $|\exp(j\alpha_{k,n})| = 1$ and $\alpha_{k,n} \in [0, 2\pi)$. To solve (36), we have

$$|\mathbf{h}_k \Theta_k \mathbf{h}_r + h_{d,k}| = |\theta_k \mathbf{b}_k + h_{d,k}|, \quad (37)$$

where $\mathbf{b}_k = \text{diag}(\mathbf{h}_k) \mathbf{h}_r$, $\theta_k = [\theta_{k,1}, \dots, \theta_{k,N_R}] = [\exp(j\alpha_{k,1}), \dots, \exp(j\alpha_{k,N_R})]$, $|\theta_{k,n}| = 1$. To proceed, we apply the triangle inequality to the right hand side (RHS) of (37) to achieve its upper bound, which aims to obtain the optimal phase shifts of the WIT phase θ_k in problem (37) [54]. As such, the upper bound of (37) is given as

$$|\theta_k \mathbf{b}_k + h_{d,k}| \leq \sum_{n=1}^{N_R} |\theta_{k,n} \mathbf{b}_k[n]| + |h_{d,k}| = \sum_{n=1}^{N_R} |\mathbf{b}_k[n]| + |h_{d,k}|, \quad (38)$$

where $\mathbf{b}_k[n]$ is the n -th element of \mathbf{b}_k , and equality holds with $|\theta_{k,n}| = 1$ for $n \in [1, N_R]$. According to [54], the upper bound in (38) can be obtained via

$$\alpha_{k,n}^* = \arg(h_{d,k}) - \arg(\mathbf{b}_k[n]), \quad \text{and} \quad \theta_{k,n}^* = \exp(j\alpha_{k,n}). \quad (39)$$

Thus, the optimal phase shifts of the WIT is derived by θ_k^* in (39), and equivalently the optimal solution to (36) (i.e., Θ_k^*) is obtained from θ_k^* . Thus, we complete the proof of *Theorem 1*.

B. Proof of Lemma 1

We exploit a few of mathematical manipulations to expand the term $|\mathbf{h}_k \Theta_k^* \mathbf{h}_r + h_{d,k}|^2$,

$$|\mathbf{h}_k \Theta_k^* \mathbf{h}_r + h_{d,k}|^2 = |\mathbf{h}_k \Theta_k^* \mathbf{h}_r|^2 + |h_{d,k}|^2 + 2|\mathbf{h}_k \Theta_k^* \mathbf{h}_r| |h_{d,k}| \cos(\arg(h_{d,k}) - \arg(\mathbf{h}_k \Theta_k^* \mathbf{h}_r)), \quad (40)$$

From (40), the term $|\mathbf{h}_k \Theta_k^* \mathbf{h}_r + h_{d,k}|^2$ obtains its maximum value if

$$\cos(\arg(h_{d,k}) - \arg(\mathbf{h}_k \Theta_k^* \mathbf{h}_r)) = 1. \quad (41)$$

(41) indicates that the phases of both direct and reflecting links between the k -th sensor node and the AP are identical, i.e., $\arg(h_{d,k}) = \arg(\mathbf{h}_k \Theta_k^* \mathbf{h}_r)$, which completes the proof of *Lemma 1*.

C. Proof of Lemma 2

The objective function (12a) is an increasing function with respect to P_k and τ_k , $\forall k \in [1, K]$. Thus, the constraints (12b) and (3) are satisfied with equality when the optimal solutions to problem (12) are achieved. From the constraint (3), it is readily observed that its RHS is monotonically increasing with respect to $t_{0,1}$. As such, the constraint (6d) holds the equality with the optimal solution, otherwise it is always required to increase $t_{0,1}$ such that $t_{0,2}$ and the harvested energy of the IoT sensors can also be increased until the equality holds. Similarly, the equality holds in the constraint (6e) with the optimal solution, otherwise it requires increasing τ_0 , leading to the increase of $t_{0,i}$ until equality holds. Thus, the following equalities hold with the optimal solution:

$$\tau_k^* P_k^* = t_{0,1}^* \eta P_0 |g_{d,k}|^2 + t_{0,2}^* \eta P_0 |\mathbf{g}_0 \Theta_0^* \mathbf{g}_{r,k} + g_{d,k}|^2, \quad (42a)$$

$$N_R P_{c,IRS} \left(t_{0,2}^* + \sum_{k=1}^K \tau_k^* \right) = t_{0,1}^* \eta P_0 \|\mathbf{g}_0\|^2, \quad (42b)$$

$$\sum_{i=1}^2 t_{0,i}^* = \tau_0^*, \quad (42c)$$

$$\sum_{k=0}^K \tau_k^* = T, \quad (42d)$$

From (42a), (42c), and (42d), the first part of *Lemma (2)* has been proved. We substitute (13b) into (42b), and then achieve the optimal closed-form $t_{0,1}^*$ shown in (14), which completes the second part of *Lemma (2)*.

D. Proof of Theorem 2

To prove *Theorem 2*, we consider the Lagrange dual function of problem (15),

$$\mathcal{L}(t_{0,2}, \tau_k, \mu) = \sum_{k=1}^K \tau_k \log \left(1 + \frac{\tilde{c}_k (\bar{c}_k + t_{0,2} s_k)}{\tau_k} \right) - \mu \left(t_{0,1}^* + t_{0,2} + \sum_{k=1}^K \tau_k - T \right), \quad (43)$$

where $\mu \geq 0$ denotes the dual variable associate constraint (15a). Additionally, the associated dual problem to (15) is given as

$$\min_{\{t_{0,2}, \tau_k\} \in \mathcal{S}} \mathcal{L}(t_{0,2}, \tau_k, \mu), \quad (44)$$

where \mathcal{S} is the feasible set of any $t_{0,2}$ and τ_k , $\forall k \in [1, K]$, and has been shown in the constraints (15a) and (15b). As mentioned earlier, (15) can be relaxed into a convex problem that satisfies Slater's condition. Thus, the strong duality holds between (15) and (44) such that the optimal solution to (15) satisfies the KKT conditions, which is given by

$$\mu^* \left(t_{0,1}^* + t_{0,2}^* + \sum_{k=1}^K \tau_k^* - T \right) = 0, \quad (45a)$$

$$\frac{\partial \mathcal{L}}{\partial \tau_k} = 0. \quad (45b)$$

From (45a), we have $\mu > 0$ due to $\sum_{i=1}^2 t_{0,i}^* + \sum_{k=1}^K \tau_k^* = T$ from (13b). In addition, we exploit (45b) to have

$$\log \left(1 + \frac{\tilde{c}_k (\bar{c}_k + t_{0,2} s_k)}{\tau_k} \right) - \frac{\tilde{c}_k (\bar{c}_k + t_{0,2} s_k)}{\tau_k + \tilde{c}_k (\bar{c}_k + t_{0,2} s_k)} = \mu. \quad (46)$$

The equality (46) is similar to the form $f(x) = \log(1+x) + \frac{x}{1+x}$ which is a monotonically increasing function with respect to x . Thus, in order to satisfy the above K equations in (46), we have

$$\frac{\tilde{c}_1 (\bar{c}_1 + t_{0,2} s_1)}{\tau_1} = \dots = \frac{\tilde{c}_K (\bar{c}_K + t_{0,2} s_K)}{\tau_K} \quad (47)$$

Denoting $\frac{\tilde{c}_k (\bar{c}_k + t_{0,2} s_k)}{\tau_k} = \frac{1}{r}$, we have

$$\tau_k = r \tilde{c}_k (\bar{c}_k + t_{0,2} s_k). \quad (48)$$

By substituting (48) into (15a), we obtain

$$r = \frac{T - t_{0,1}^* - t_{0,2}}{\sum_{k=1}^K \tilde{c}_k (\bar{c}_k + t_{0,2} s_k)}. \quad (49)$$

We substitute (49) into (48) to complete the proof of *Theorem 2*.

E. Proof of Theorem 3

To solve (22), we approximate its objective function via the MM algorithm.

Proposition 1: [51] The objective function (22a) is approximately written, for any given $\boldsymbol{\theta}^{(m)}$ at the m -th iteration and for any feasible $\boldsymbol{\theta}_0$, as

$$\begin{aligned} f(\boldsymbol{\theta}_0) &= \boldsymbol{\theta}_0 \boldsymbol{\Phi} \boldsymbol{\theta}_0^H - 2\Re\{\boldsymbol{\theta}_0 \boldsymbol{\gamma}\} + d \\ &\leq \boldsymbol{\theta}_0 \boldsymbol{\Upsilon} \boldsymbol{\theta}_0^H - 2\Re\left\{ \boldsymbol{\theta}_0 \left[(\boldsymbol{\Upsilon} - \boldsymbol{\Phi}) \tilde{\boldsymbol{\theta}}_0^H + \boldsymbol{\gamma} \right] \right\} \\ &\quad + \tilde{\boldsymbol{\theta}}_0 (\boldsymbol{\Upsilon} - \boldsymbol{\Phi}) \tilde{\boldsymbol{\theta}}_0^H + d \\ &= \lambda_{\max}(\boldsymbol{\Phi}) \|\boldsymbol{\theta}_0\|^2 - 2\Re\left\{ \boldsymbol{\theta}_0 \left[(\lambda_{\max}(\boldsymbol{\Phi}) \mathbf{I}_{N \times N} - \boldsymbol{\Phi}) \tilde{\boldsymbol{\theta}}_0^H \right. \right. \\ &\quad \left. \left. + \boldsymbol{\gamma} \right] \right\} + \tilde{d} = g(\boldsymbol{\theta} | \boldsymbol{\theta}^{(m)}), \end{aligned} \quad (50)$$

where $\tilde{d} = \tilde{\boldsymbol{\theta}}_0 [\lambda_{\max}(\boldsymbol{\Phi}) \mathbf{I}_{N_R \times N_R} - \boldsymbol{\Phi}] \tilde{\boldsymbol{\theta}}_0^H + d$, and $\boldsymbol{\Upsilon} = \lambda_{\max}(\boldsymbol{\Phi}) \mathbf{I}_{N_R \times N_R}$.

Proposition 1 constructs a surrogate function of (22a), and it is easily verified that $g(\boldsymbol{\theta} | \boldsymbol{\theta}^{(m)})$ in (50) guarantees the conditions in (25).

$$\begin{aligned} \min_{\boldsymbol{\theta}_0} \lambda_{\max}(\boldsymbol{\Phi}) \|\boldsymbol{\theta}_0\|^2 - 2\Re\{\boldsymbol{\theta}_0 \tilde{\boldsymbol{\gamma}}\} \\ \text{s.t. } |\boldsymbol{\theta}_0(n)| = 1, \forall n \in [1, N_R]. \end{aligned} \quad (51)$$

It is clearly seen that $\|\boldsymbol{\theta}_0\|^2 = N_R$ due to $|\boldsymbol{\theta}_0(n)| = 1$. The term $\Re\{\boldsymbol{\theta}_0 \tilde{\boldsymbol{\gamma}}\}$ can be maximized when the phases of $\boldsymbol{\theta}_0(n)$ and $\tilde{\boldsymbol{\gamma}}(n)$ are identical. We complete the proof of *Theorem 3*.

F. Proof of Theorem 4

To prove *Theorem 4*, we first rewrite the objective function (17a) with respect to $t_{0,2}$ as

$$f(t_{0,2}) = (\tilde{T} - t_{0,2}) \log \left(1 + \frac{c + t_{0,2}s}{\tilde{T} - t_{0,2}} \right) \quad (52)$$

Considering the first-order derivative of (52) and setting it to zero, we have the following equality

$$x \log(x) - x = s^* - 1, \quad (53)$$

where $x = 1 + \frac{c+t_{0,2}s}{\tilde{T}-t_{0,2}}$. With some mathematical manipulations, (53) can be expressed equivalently as

$$\log \left(\frac{x}{\exp(1)} \right) \exp \left[\log \left(\frac{x}{\exp(1)} \right) \right] = \frac{s-1}{\exp(1)}, \quad (54)$$

Applying the relation $z \exp(z) = y \Rightarrow z = \mathcal{W}(y)$ into (54), we complete the proof of *Theorem 4*.

G. Proof of Theorem 5

To prove *Theorem 5*, the Lagrange dual function of (32) is applied,

$$\begin{aligned} \mathcal{L}(t_{0,2}, \tau_k, \mu_1) &= \sum_{k=1}^K \tau_k \log \left(1 + \frac{a_k + t_{0,2}b_k}{\tau_k} - d_k \right) \\ &\quad - \mu_1 \left(t_{0,1}^* + t_{0,2} + \sum_{k=1}^K \tau_k - T \right), \end{aligned} \quad (55)$$

where μ_1 denotes the dual multiplier associated with constraint (32b). Taking the first-order partial derivative of this dual function with respect to $t_{0,2}$ and τ_k , respectively, we have

$$\frac{\partial \mathcal{L}}{\partial t_{0,2}} = \sum_{k=1}^K \frac{b_k}{1 + x_k - d_k} - \mu_1, \quad (56a)$$

$$\frac{\partial \mathcal{L}}{\partial \tau_k} = \log(1 + x_k - d_k) - \frac{x_k}{1 + x_k - d_k} - \mu_1, \quad (56b)$$

where $x_k = \frac{a_k + t_{0,2}b_k}{\tau_k}$, $\forall k \in [1, K]$. To obtain the optimal closed-form solution of $t_{0,2}$ and τ_k , $\forall k \in [1, K]$, we let $\frac{\partial \mathcal{L}}{\partial t_{0,2}} = 0$ and $\frac{\partial \mathcal{L}}{\partial \tau_k} = 0$, $\forall k \in [1, K]$, respectively. Consequently, the optimal solution x_k^* can be obtained via solving the following equation

$$\log(1 + x_k - d_k) - \frac{x_k}{1 + x_k - d_k} = \sum_{k=1}^K \frac{b_k}{1 + x_k - d_k}, \forall k \in [1, K],$$

which can be efficiently obtained by numerical methods, e.g., bisection method. Then, the constraint (32b) holds with equality at the optimal solution, and we have

$$t_{0,1}^* + t_{0,2} + \sum_{k=1}^K \frac{a_k + t_{0,2}b_k}{x_k^*} = T. \quad (57)$$

Hence, the optimal closed-form time, $t_{0,2}^*$ and τ_k , $\forall k \in [1, K]$ can be derived as (33). This completes the proof of *Theorem 5*.

REFERENCES

- [1] M. Zhong, Y. Yang, H. Yao, X. Fu, O. A. Dobre, and O. Postolache, "5G and IoT: Towards a new era of communications and measurements," *IEEE Instrum. Meas. Mag.*, vol. 22, no. 6, pp. 18–26, 2019.
- [2] Q. Wu, G. Y. Li, W. Chen, D. W. K. Ng, and R. Schober, "An overview of sustainable green 5G networks," *IEEE Wireless Commun.*, vol. 24, no. 4, pp. 72–80, Aug. 2017.
- [3] X. Chen, D. W. K. Ng, W. Yu, E. G. Larsson, N. Al-Dhahir, and R. Schober, "Massive access for 5G and beyond," *to appear in IEEE J. Sel. Areas Commun.*, 2020.
- [4] Z. Chu, F. Zhou, Z. Zhu, R. Q. Hu, and P. Xiao, "Wireless powered sensor networks for internet of things: Maximum throughput and optimal power allocation," *IEEE Internet Things J.*, vol. 5, no. 1, pp. 310–321, Feb. 2018.
- [5] R. Zhang and C. K. Ho, "MIMO broadcasting for simultaneous wireless information and power transfer," *IEEE Trans. Wireless Commun.*, vol. 12, no. 5, pp. 1989–2001, May 2013.
- [6] L. R. Varshney, "Transporting information and energy simultaneously," in *Proc. IEEE ISIT, Toronto, ON, Canada*, pp. 1612–1616, 2008.
- [7] K. Huang and X. Zhou, "Cutting the last wires for mobile communications by microwave power transfer," *IEEE Commun. Mag.*, vol. 53, no. 6, pp. 86–93, Jun. 2015.
- [8] B. Clerckx, R. Zhang, R. Schober, D. W. K. Ng, D. I. Kim, and H. V. Poor, "Fundamentals of wireless information and power transfer: From rf energy harvester models to signal and system designs," *IEEE J. Sel. Areas Commun.*, vol. 37, no. 1, pp. 4–33, Jan. 2019.
- [9] S. Bi, C. K. Ho, and R. Zhang, "Wireless powered communication: opportunities and challenges," *IEEE Commun. Mag.*, vol. 53, no. 4, pp. 117–125, Apr. 2015.
- [10] S. Bi, Y. Zeng, and R. Zhang, "Wireless powered communication networks: an overview," *IEEE Wireless Commun.*, vol. 23, no. 2, pp. 10–18, Apr. 2016.
- [11] H. Ju and R. Zhang, "Throughput maximization in wireless powered communication networks," *IEEE Trans. Wireless Commun.*, vol. 13, no. 1, pp. 418–428, Jan. 2014.
- [12] Z. Gao, L. Dai, D. Mi, Z. Wang, M. A. Imran, and M. Z. Shakir, "MmWave massive-MIMO-based wireless backhaul for the 5G ultra-dense network," *IEEE Wireless Commun.*, vol. 22, no. 5, pp. 13–21, Oct. 2015.
- [13] X. Chen, C. Zhong, C. Yuen, and H. Chen, "Multi-antenna relay aided wireless physical layer security," *IEEE Commun. Mag.*, vol. 53, no. 12, pp. 40–46, Dec. 2015.
- [14] S. Chen, F. Qin, B. Hu, X. Li, and Z. Chen, "User-centric ultra-dense networks for 5G: challenges, methodologies, and directions," *IEEE Wireless Commun.*, vol. 23, no. 2, pp. 78–85, Apr. 2016.
- [15] Renzo, Marco Di, et. al., "Smart radio environments empowered by reconfigurable AI meta-surfaces: an idea whose time has come," *EURASIP J. Wirel. Commun. Netw.*, no. 129, pp. 1–20, May 2019.
- [16] M. D. Renzo, A. Zappone, M. Debbah, M. Alouini, C. Yuen, J. D. Rosny, and S. Tretjakov, "Smart radio environments empowered by reconfigurable intelligent surfaces: How it works, state of research, and road ahead," *to appear in IEEE J. Sel. Areas Commun.*, 2020.
- [17] C. Huang, S. Hu, G. C. Alexandropoulos, A. Zappone, C. Yuen, R. Zhang, M. Di Renzo, and M. Debbah, "Holographic MIMO surfaces for 6G wireless networks: Opportunities, challenges, and trends," *to appear in IEEE Wireless Commun.*, 2020.
- [18] Q. Wu and R. Zhang, "Towards smart and reconfigurable environment: Intelligent reflecting surface aided wireless network," *IEEE Commun. Mag.*, vol. 58, no. 1, pp. 106–112, Jan. 2020.
- [19] S. Hu, F. Rusek, and O. Edfors, "Beyond massive MIMO: The potential of positioning with large intelligent surfaces," *IEEE Trans. Signal Process.*, vol. 66, no. 7, pp. 1761–1774, Apr. 2018.
- [20] Q. Wu and R. Zhang, "Intelligent reflecting surface enhanced wireless network via joint active and passive beamforming," *IEEE Trans Wireless Commun.*, vol. 18, no. 11, pp. 5394–5409, Nov. 2019.
- [21] C. Huang, A. Zappone, G. C. Alexandropoulos, M. Debbah, and C. Yuen, "Reconfigurable intelligent surfaces for energy efficiency in wireless communication," *IEEE Trans. Wireless Commun.*, vol. 18, no. 8, pp. 4157–4170, Aug. 2019.
- [22] Z. Chu, W. Hao, P. Xiao, and J. Shi, "Intelligent reflecting surface aided multi-antenna secure transmission," *IEEE Wireless Commun. Lett.*, vol. 9, pp. 108–112, Jan 2020.
- [23] H. Shen, W. Xu, S. Gong, Z. He, and C. Zhao, "Secrecy rate maximization for intelligent reflecting surface assisted multi-antenna communications," *IEEE Commun. Lett.*, vol. 23, no. 9, pp. 1488–1492, Sep. 2019.
- [24] X. Guan, Q. Wu, and R. Zhang, "Intelligent reflecting surface assisted secrecy communication: Is artificial noise helpful or not?," *IEEE Wireless Commun. Lett.*, vol. 9, no. 6, pp. 778–782, Jun. 2020.

- [25] C. Pan, H. Ren, K. Wang, W. Xu, M. ElKashlan, A. Nallanathan, and L. Hanzo, "Multicell MIMO communications relying on intelligent reflecting surfaces," *IEEE Trans. Wireless Commun.*, vol. 19, no. 8, pp. 5218–5233, Aug. 2020.
- [26] G. Zhou, C. Pan, H. Ren, K. Wang, and A. Nallanathan, "Intelligent reflecting surface aided multigroup multicast MISO communication systems," *IEEE Trans. Signal Process.*, vol. 68, pp. 3236–3251, Apr. 2020.
- [27] Q. Wu and R. Zhang, "Weighted sum power maximization for intelligent reflecting surface aided SWIPT," *IEEE Wireless Commun. Lett.*, vol. 9, no. 5, pp. 586–590, May 2020.
- [28] Q. Wu and R. Zhang, "Joint active and passive beamforming optimization for intelligent reflecting surface assisted SWIPT under QoS constraints," *IEEE J. Sel. Areas Commun.*, vol. 38, no. 8, pp. 1735–1748, Aug. 2020.
- [29] C. Pan, H. Ren, K. Wang, M. ElKashlan, A. Nallanathan, J. Wang, and L. Hanzo, "Intelligent reflecting surface aided MIMO broadcasting for simultaneous wireless information and power transfer," *IEEE J. Sel. Areas Commun.*, vol. 38, no. 8, pp. 1719–1734, Aug. 2020.
- [30] W. Hao, G. Sun, M. Zeng, Z. Zhu, Z. Chu, O. A. Dobre, and P. Xiao, "Robust design for intelligent reflecting surface assisted MIMO-OFDMA terahertz communications," <https://arxiv.org/abs/2009.05893>, 2020.
- [31] H. Ibrahim, H. Tabassum, and U. T. Nguyen, "Exact coverage analysis of intelligent reflecting surfaces with nakagami-m channels," <https://arxiv.org/abs/2101.00740>, 2021.
- [32] S. Zarandi and H. Tabassum, "Delay minimization in sliced multi-cell mobile edge computing (MEC) systems," <https://arxiv.org/abs/2101.03405>, 2021.
- [33] E. Bjornson, O. Ozdogan, and E. G. Larsson, "Reconfigurable intelligent surfaces: Three myths and two critical questions," *IEEE Commun. Mag.*, vol. 58, no. 12, pp. 90–96, Dec. 2020.
- [34] Y. Hu, X. Yuan, T. Yang, B. Clerckx, and A. Schmeink, "On the convex properties of wireless power transfer with nonlinear energy harvesting," *IEEE Trans. Vehicular Technol.*, vol. 69, no. 5, pp. 5672–5676, May 2020.
- [35] S. Shen and B. Clerckx, "Joint waveform and beamforming optimization for MIMO wireless power transfer," <https://arxiv.org/abs/2009.07500>, 2020.
- [36] L. Irio, R. Oliveira, D. B. da Costa, and M. Alouini, "Impact of wireless-powered communications in coexisting mobile networks," *IEEE Wireless Commun. Lett.*, vol. 9, no. 7, pp. 1060–1064, Jul. 2020.
- [37] M. Gharbieh, H. ElSawy, M. Emara, H. C. Yang, and M. S. Alouini, "Grant-free opportunistic uplink transmission in wireless-powered IoT: A spatio-temporal model," *IEEE Transactions on Communications*, vol. 69, no. 2, pp. 991–1006, Feb. 2021.
- [38] B. Clerckx, K. Huang, L. R. Varshney, S. Ulukus, and M.-S. Alouini, "Wireless power transfer for future networks: Signal processing, machine learning, computing, and sensing," <https://arxiv.org/abs/2101.04810>, 2021.
- [39] Z. Wang, Y. Shi, Y. Zhou, H. Zhou, and N. Zhang, "Wireless-powered over-the-air computation in intelligent reflecting surface aided IoT networks," to appear in *IEEE Internet Things J.*, pp. 1–1, 2020.
- [40] B. Lyu, P. Ramezani, D. T. Hoang, S. Gong, Z. Yang, and A. Jamalipour, "Optimized energy and information relaying in self-sustainable IRS-empowered WPCN," <https://arxiv.org/abs/2004.03108v1>, 2020.
- [41] Q. Wu, M. Tao, D. W. Kwan Ng, W. Chen, and R. Schober, "Energy-efficient resource allocation for wireless powered communication networks," *IEEE Trans. Wireless Commun.*, vol. 15, no. 3, pp. 2312–2327, Mar. 2016.
- [42] H. Ju and R. Zhang, "Throughput maximization in wireless powered communication networks," *IEEE Trans. Wireless Commun.*, vol. 13, no. 1, pp. 418–428, Jan. 2014.
- [43] Z. Wang, L. Liu, and S. Cui, "Channel estimation for intelligent reflecting surface assisted multiuser communications: Framework, algorithms, and analysis," *IEEE Trans. Wireless Commun.*, vol. 19, no. 10, pp. 6607–6620, Oct. 2020.
- [44] Y. Omid, S. M. M. Shahabi, C. Pan, Y. Deng, and A. Nallanathan, "PDD-based robust beamforming design for IRS-aided MISO systems with imperfect channels," <https://arxiv.org/abs/2008.10699>, 2020.
- [45] S. Hong, C. Pan, H. Ren, K. Wang, K. K. Chai, and A. Nallanathan, "Robust transmission design for intelligent reflecting surface aided secure communication systems with imperfect cascaded CSI," to appear in *IEEE Trans. Wireless Commun.*, pp. 1–1, 2020.
- [46] G. Zhou, C. Pan, H. Ren, K. Wang, and A. Nallanathan, "A framework of robust transmission design for IRS-aided MISO communications with imperfect cascaded channels," *IEEE Trans. Signal Process.*, vol. 68, pp. 5092–5106, Aug. 2020.
- [47] Q. Wu and R. Zhang, "Beamforming optimization for wireless network aided by intelligent reflecting surface with discrete phase shifts," *IEEE Trans. Commun.*, vol. 68, no. 3, pp. 1838–1851, Mar. 2020.
- [48] O. Ozdogan, E. Bjornson, and E. G. Larsson, "Intelligent reflecting surfaces: Physics, propagation, and pathloss modeling," *IEEE Wireless Commun. Lett.*, vol. 9, no. 5, pp. 581–585, May 2020.
- [49] S. Boyd and L. Vandenberghe, *Convex Optimization*. Cambridge, UK: Cambridge University Press, 2004.
- [50] Y. Sun, P. Babu, and D. P. Palomar, "Majorization-minimization algorithms in signal processing, communications, and machine learning," *IEEE Trans. Signal Process.*, vol. 65, no. 3, pp. 794–816, Feb. 2017.
- [51] J. Song, P. Babu, and D. P. Palomar, "Sequence design to minimize the weighted integrated and peak sidelobe levels," *IEEE Trans. Signal Process.*, vol. 64, no. 8, pp. 2051–2064, Apr. 2016.
- [52] Q. Wu, W. Chen, D. W. K. Ng, and R. Schober, "Spectral and energy-efficient wireless powered IoT networks: NOMA or TDMA?," *IEEE Trans. Veh. Technol.*, vol. 67, no. 7, pp. 6663–6667, 2018.
- [53] N. Shafiee, S. Tewari, B. Calhoun, and A. Shrivastava, "Infrastructure circuits for lifetime improvement of ultra-low power IoT devices," *IEEE Transactions on Circuits and Systems I: Regular Papers*, vol. 64, no. 9, pp. 2598–2610, 2017.
- [54] Y. Zheng, S. Bi, Y. J. Zhang, Z. Quan, and H. Wang, "Intelligent reflecting surface enhanced user cooperation in wireless powered communication networks," *IEEE Wireless Commun. Lett.*, vol. 9, no. 6, pp. 901–905, Jun. 2020.